Electronic Supplementary Material (ESI) for ChemComm.

Acidochromism of Donor Acceptor Stenhouse Adducts in Organic Solvent

Antonio Fiorentino,[a] Brian Sachini,[b] Stefano Corra,[b,c] Alberto Credi,[b,c] Cristina Femoni,[c] Aurore Fraix,[d] and Serena Silvi*[a,b]

[a.] Dipartimento di Chimica "G. Ciamician", Università di Bologna, via Selmi 2, 40126 Bologna.

[b.] CLAN-Center for Light Activated Nanostructures, Istituto ISOF-CNR, via Gobetti 101, 40129 Bologna, Italy.

[c.] Dipartimento di Chimica Industriale "Toso Montanari", Università di Bologna, Viale del Risorgimento 4, 40136 Bologna, Italy.

[d.] PhotoChemLab, Department of Drug and Health Sciences, University of Catania, 95125 Catania, Italy.

SUPPLEMENTARY INFORMATION

1. Materials and methods

General Materials. All solvents and chemicals were purchased from Sigma-Aldrich, Fluorochem, or VWR international and were used as received. In reactions where water was the solvent, Milli-Q water was used. Reactions were monitored by thin layer chromatography (TLC) performed on TLC Silica gel 60 F254 coated aluminium plates purchased from Merck. Flash column chromatography was performed using Sigma-Aldrich Silica 40 (230-400 mesh size or 40-63 mm) as the stationary phase.

NMR Spectroscopy. Nuclear magnetic spectroscopy (NMR) spectra were recorded on an Agilent DD2 spectrometer operating at 500 MHz or on a Varian Mercury 400 MHz spectrometer operating at 400 MHz. Chemical shifts (δ) are quoted in ppm relative to tetramethylsilane using the residual signal of the deuterated solvent as reference (CD_3Cl: ^1H δ = 7.26 ppm and CD_2Cl_2: ^1H δ = 5.32 ppm). Coupling constants (J) are expressed in Hertz (Hz) and refer to H–H coupling unless otherwise stated. Multiplicities were reported as follows: s = singlet, d = doublet, t = triplet, q = quartet, dd = doublets of doublets, ddd = doublets of doublets of doublets, td = triplets of doublets. In case no multiplicity could be identified, the chemical shift range of the signal is given as m = multiplet.

X-ray Crystallography. Single-crystal X-ray diffraction experiments were performed at 100 K or room temperature, on a Bruker Apex II diffractometer, equipped with a Complementary Metal Oxide Semiconductor (CMOS) area detector, by using Kα-Mo radiation. Data were corrected for Lorentz polarization and absorption effects (empirical absorption correction SADABS).[1] Structures were solved by direct methods and refined by full-matrix least-squares based on all data using F^2.[2] All hydrogen atoms were fixed at calculated positions and refined by a riding model. All non-hydrogen atoms were refined with anisotropic displacement parameters, including disordered atoms. In the case of compound **1b**-H^+, the F and O atoms in the triflate anion were split in two positions, as well as the ethyl groups coordinated to the N atom of the ammonium group. Therefore, in order to obtain a better structural model, geometrical and anisotropic parameter restraints were applied. In the case of compound **2b**-H^+, the diffraction power of its crystal at high theta value was rather low, and this accounts for the unique Alert_B after the cif check. Note that a complete set of data was collected for both compounds, irrespective of their crystal system.

Structure drawings were made with SCHAKAL99 software[3] and ORTEP. CCDC 2181185-2181186 contain the supplementary crystallographic data for compounds **2b**-H^+ and **1b**-H^+, respectively.

Absorption and emission measurements. All the absorption spectra were collected in the UV-visible range on spectrophotometers Varian Cary 300 (double beam) or Varian Cary 50 bio (single beam). For the measurements quartz cuvettes with 1 cm pathlength were used. All the luminescence spectra were collected on an Edinburgh Instruments FS5 spectrofluorometer. Emission quantum yields were evaluated using the relative method, according to the law:[4]

$$\Phi = \Phi_s \times \frac{A_s}{A} \times \frac{I}{I_s} \times \frac{n^2}{n_s^2} \qquad \textbf{Eq. 1}$$

where the subscript "s" indicates the standard, which in the case of this work was an aerated solution of $[Ru(bpy)_3]Cl_2$ in H_2O ($\Phi_{EM} = 0.040$);[5] *A* is at the excitation wavelength, *I* the integrated emission value and *n* the refractive index of the solvent. In order to avoid any correction, an isoabsorbance point was chosen as excitation wavelength.

Spectrophotometric titrations and kinetic experiments. Spectroscopic titrations were conducted by adding small amounts (1-500 µL) of concentrated acid or base solutions to diluted solutions of DASAs and recording the corresponding absorption spectrum after equilibrium was achieved. Obtained data were then fitted using the HYPERQUAD suite, which allows a global analysis of the spectra and provides the corresponding thermodynamic constant related to the process.[6] Cyclization and ring-opening processes were investigated monitoring the absorption variations over time in the dark and fitting the obtained data with the software OriginPro.

Irradiation measurements. Irradiation experiments were performed on air-equilibrated solutions, thoroughly stirred at room temperature. A Helios Italquartz Polymer Hg medium pressure lamp (125 W) was used as light source, equipped with a cut-off filter > 399 nm to irradiate in the visible range. The incident photon flux of the lamp in these conditions was estimated to be 3×10^{-7} E s^{-1} by means of the potassium reineckate actinometer.[7]

Numerical simulations. Numerical simulation of the acidochromism model was performed using the software Berkeley Madonna 10.[8] The simulation was performed implementing the kinetic model as a system of differential equations that was solved numerically by the software.

2. Synthetic procedures

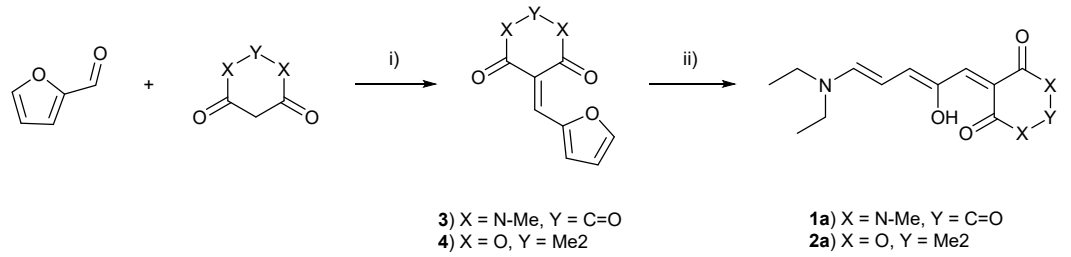

Scheme 1: General synthetic route towards DASAs **1a** and **2a**. i) compound **3**: H_2O, room temperature, 2 h; compound **4**: H_2O, 75 °C, 2 h. ii) Diethylamine, THF, room temperature, 30 min.

General procedure for the synthesis of acceptors 3 and 4.

Acceptors **3** and **4** were synthesized according to previously reported procedures.[9]

1,3-dimethylbarbituric acid (0.81 g, 5.20 mmol) or Meldrum's acid (0.75 g, 5.20 mmol) and furfural (0.50 g, 5.20 mmol, 0.43 mL) were suspended in 15 mL H_2O. The heterogeneous mixture was stirred at room temperature for acceptor **3** or at 75 °C for **4**. Stirring was continued until complete consumption of the starting materials as monitored by TLC (3/1 hexane/ethyl acetate). During the course of the reaction a yellow precipitate formed which was collected by vacuum filtration and washed twice with cold H_2O. The collected solid was dissolved in dichloromethane (15 mL), washed with 15 mL aqueous $NaHSO_3$ (saturated, 15 mL), H_2O (15 mL), aqueous $NaHCO_3$ (saturated, 15 mL), and brine (15 mL). The organic layer was dried over $MgSO_4$, and the solvent removed under vacuum to afford the desired compound which was used in crude purity.

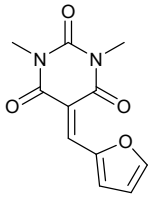

Acceptor **3**: bright yellow solid (1.12 g, 4.77 mmol, 92%). **^{1}H NMR (500 MHz, $CDCl_3$, 298K)** *δ (ppm)* 8.63 (d, *J* = 3.9 Hz, 1H), 8.43 (s, 1H), 7.85 (d, *J* = 1.9 Hz, 1H), 6.74 (dd, *J* = 3.8, 0.9 Hz, 1H), 3.40 (d, *J* = 4.0 Hz, 6H).

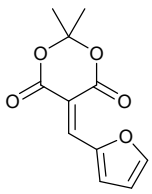

Acceptor **4**: bright yellow solid (0.71 g, 3.19 mmol, 62%). **^{1}H NMR (500 MHz, $CDCl_3$, 298K)** *δ (ppm)* 8.46 (d, *J* = 3.9 Hz, 1H), 8.35 (s, 1H), 7.84 (s, 1H), 6.75 (dd, J = 3.8, 0.9 Hz, 1H), 1.77 (s, 6H).

General procedure for the synthesis of DASA 1a and 2a.

DASA compounds **1a** and **2a** were synthesized utilizing an adaptation of previously reported procedures.[9a, 10]

Acceptor **3** (0.76 g, 3.25 mmol) or **4** (0.61 g, 3.19 mmol) were suspended in tetrahydrofuran and diethylamine (0.24 g, 3.25 mmol, 0.34 mL for **1a**, 0.23 g, 3.19 mmol, 0.33 mL for **2a**) was added. The mixture was stirred at room temperature for 30 min. The reaction mixture was, then, concentrated and the crude residue purified via flash column chromatography (SiO_2, 0 to 20% acetone in CH_2Cl_2) to afford the desired compound as a purple solid.

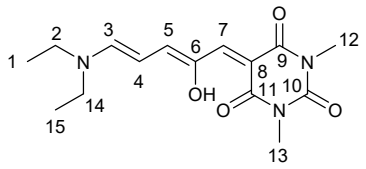

1a

DASA **1a**: purple powder (0.60 g, 1.98 mmol, 61%). Spectral data matched previous reports.[9] **^{1}H NMR (500 MHz, CD_2Cl_2, 298K)** *δ (ppm)* 12.50 (d, 0.7 Hz, 1H, O*H*), 7.28 (d, *J* = 12.3 Hz, 1H, H^3), 7.07 (s, 1H, H^7), 6.82 (dd, *J* = 12.1, 1.4 Hz, 1H, H^5), 6.10 (t, *J* = 12.3 Hz, 1H, H^4), 3.50 (dq, *J* = 21.8, 7.3 Hz, 4H, $H^{2/14}$), 3.30 (s, 3H, H^{12}), 3.27 (s, 3H, H^{13}), 1.31 (dt, *J* = 10.7, 7.3 Hz, 6H, $H^{1/15}$).

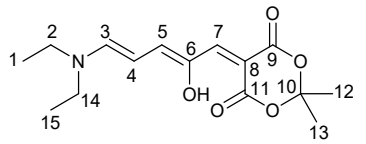

2a

DASA **2a**: purple powder (0.41 g, 1.38 mmol, 43%). Spectral data matched previous reports.[9] **^{1}H NMR (500 MHz, CD_2Cl_2, 298K)** *δ (ppm)* 11.34 (d, *J* = 0.9 Hz, 1H, OH), 7.28 (d, *J* = 12.2 Hz, 1H, H^3), 6.97 (s, 1H, H^7), 6.77 (dd, *J* = 12.5, 2.1 Hz, 1H, H^5), 6.07 (t, *J* = 12.3 Hz, 1H, H^4), 3.50 (dq, *J* = 18.3, 7.2 Hz, 4H, $H^{2/14}$), 1.68 (s, 6H, $H^{12/13}$), 1.31 (dt, *J* = 14.1, 7.3 Hz, 6H, $H^{1/15}$).

3. NMR experiments

DASA **1a** or **2a** was dissolved in deuterated dichloromethane (0.6 mL, 092 mg for **1a** and 0.88 mg for **2a**, 5 mM) inside an NMR tube. To this solution trifluoromethanesulfonic acid was added from a stock solution (0.1 M in CD_2Cl_2/CD_3CN 9:1, 30 µL, 1 equivalent). ^1H NMR spectra were recorded immediately after (Figure S1 for **1a** and S5 for **2a**). Upon protonation, clean conversion to a product which was identified as the cyclized protonated form of the DASA occurred (Figure S2 for **1a** and S6 for **2a**). The products were characterized by means of mono- and bi-dimensional NMR spectroscopy.

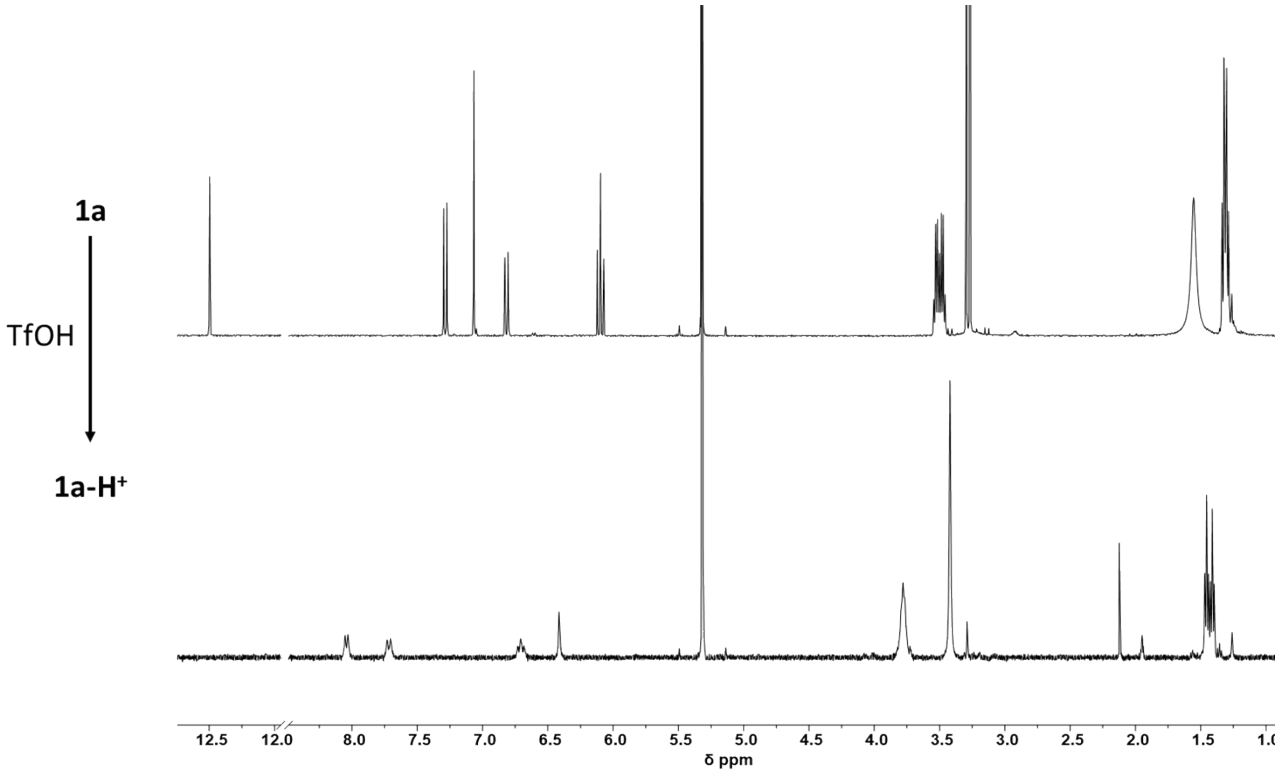

Figure S1: Stacked ^1H NMR spectra (500 MHz, CD_2Cl_2, 298 K) of a) DASA **1a** (top), b) the same sample immediately after addition of 1 equivalent of TfOH (bottom). The intensities of the resonances corresponding to the residual solvent (5.32 ppm), methyl protons 12 and 13 (3.31 and 3.24 ppm respectively) of **1a** exceed the vertical scale.

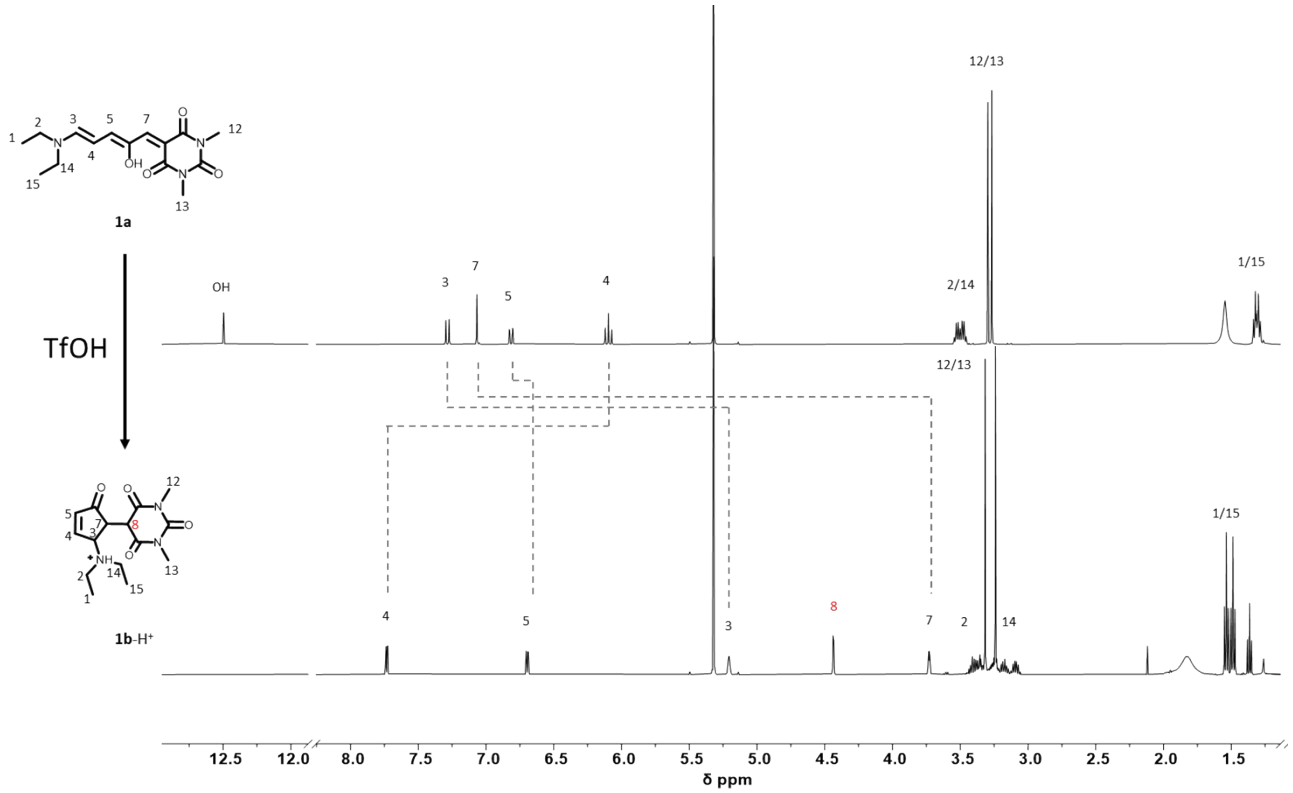

Figure S2: Stacked partial ^{1}H NMR spectra (500 MHz, CD_2Cl_2, 298 K) of a) DASA **1a** (top), b) the same sample after reaction with 1 equivalent of TfOH (bottom).

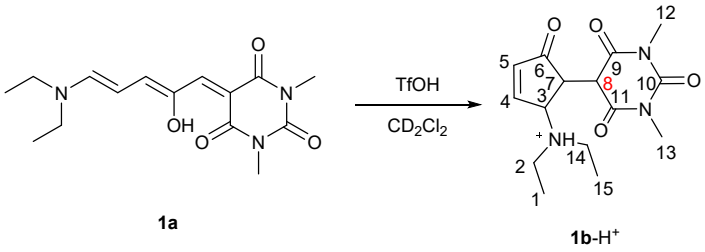

Scheme 2: Reaction of DASA **1a** with 1 equivalent of TfOH, generating cyclized DASA **1b**-H$^+$.

^{1}H NMR (500 MHz, CD_2Cl_2, 298 K) *δ (ppm)* 9.15 (s, 1H, NH), 7.74 (dd, *J* = 6.1, 2.1 Hz, 1H, H^4), 6.69 (dd, *J* = 6.0, 2.0 Hz, 1H, H^5), 5.26 – 5.08 (m, 1H, H^3), 4.44 (d, *J* = 2.1 Hz, 1H, H^8), 3.73 (dd, *J* = 4.2, 2.0 Hz, 1H, H^7), 3.46 – 3.33 (m, 3H, H^2 & H^{14}), 3.31 (s, 3H, H^{12}), 3.24 (s, 3H, H^{13}), 3.21 – 3.13 (m, 1H, H^{14}), 1.53 (t, *J* = 7.3 Hz, 3H, H^1), 1.48 (t, *J* = 7.4 Hz, 3H, H^{15}).

^{13}C NMR (126 MHz, CD_2Cl_2, 298 K) *δ* (ppm) 200.4 (C_6), 167.7 (C_9), 166.0 (C_{11}), 152.7 (C_4), 151.3 (C_{10}), 139.6 (C_5), 66.83 (C_3), 49.0 (C_2), 48.2 (C_8), 46.9 (C_{14}), 45.9 (C_7), 29.3 (C_{12}), 29.1 (C_{13}), 11.0 (C_1), 10.6 (C_{15}).

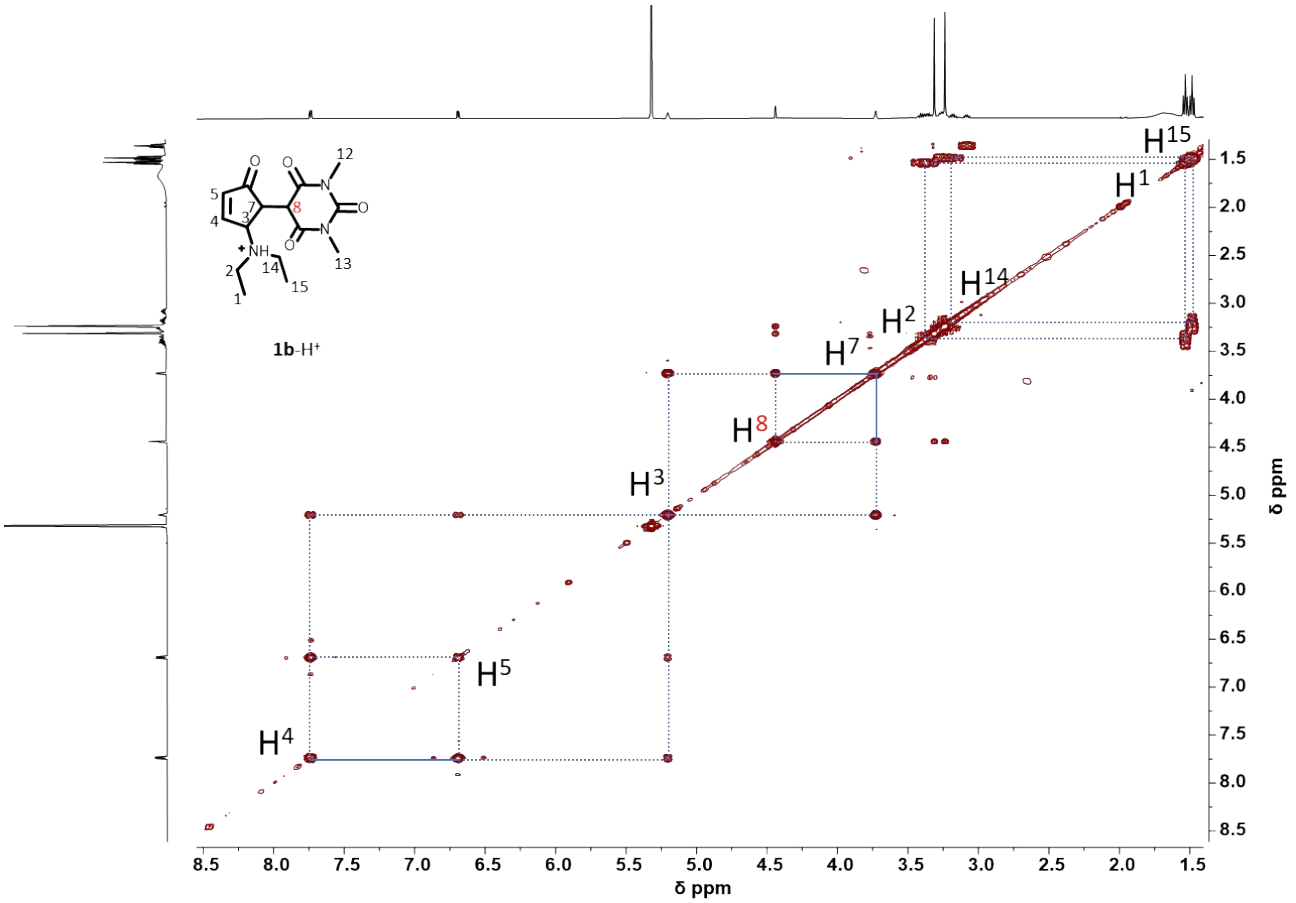

Figure S3: partial COSY spectra of **1b**-H^+. (500 MHz, CD_2Cl_2, 298 K). Cross-peaks correlating characteristic signals are highlighted with dashed squares.

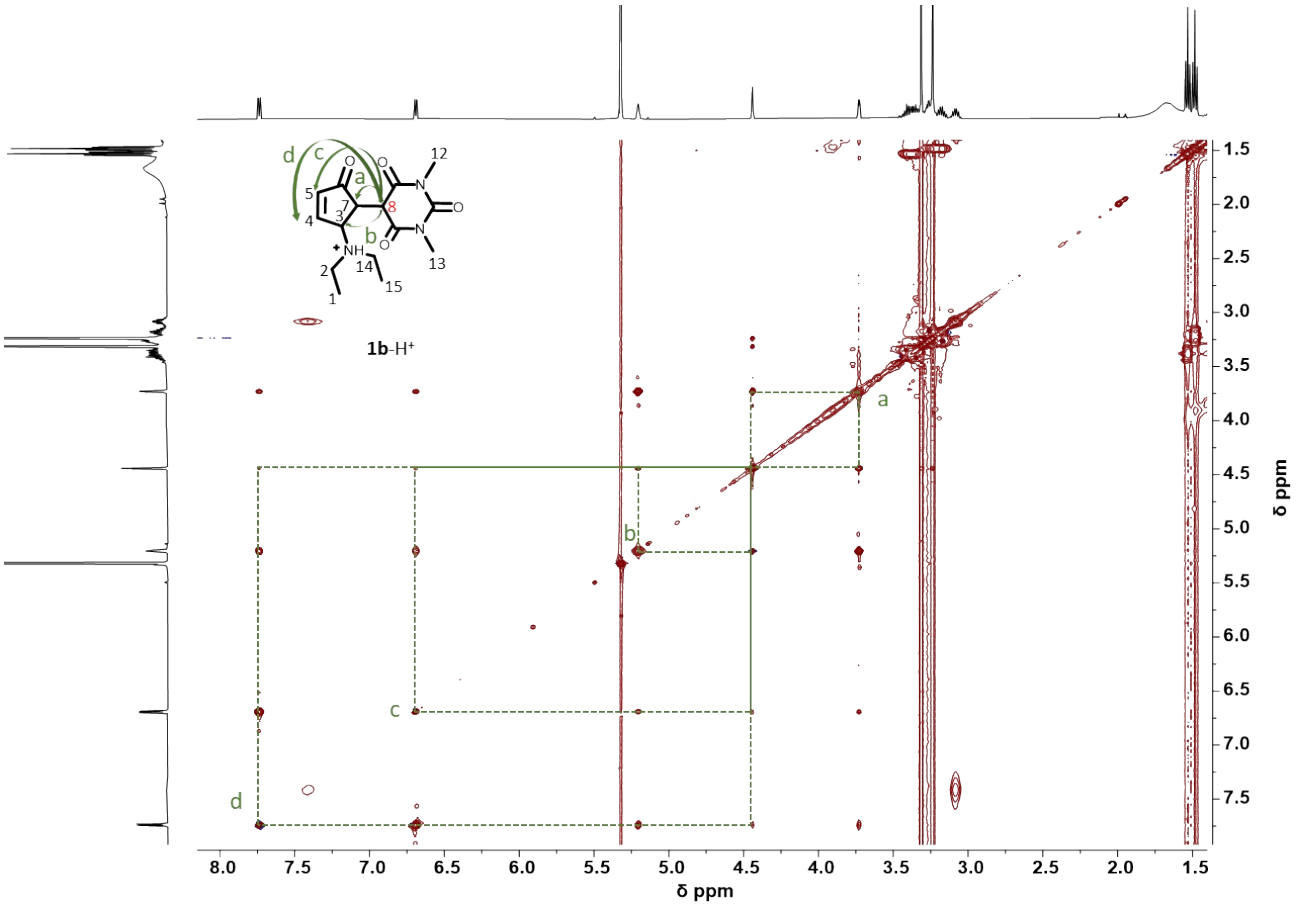

Figure S4: partial TOCSY spectra of **1b**-H⁺. (500 MHz, CD_2Cl_2, 298 K, spinlock 80 ms). Cross-peaks correlating characteristic signals are highlighted with dashed squares.

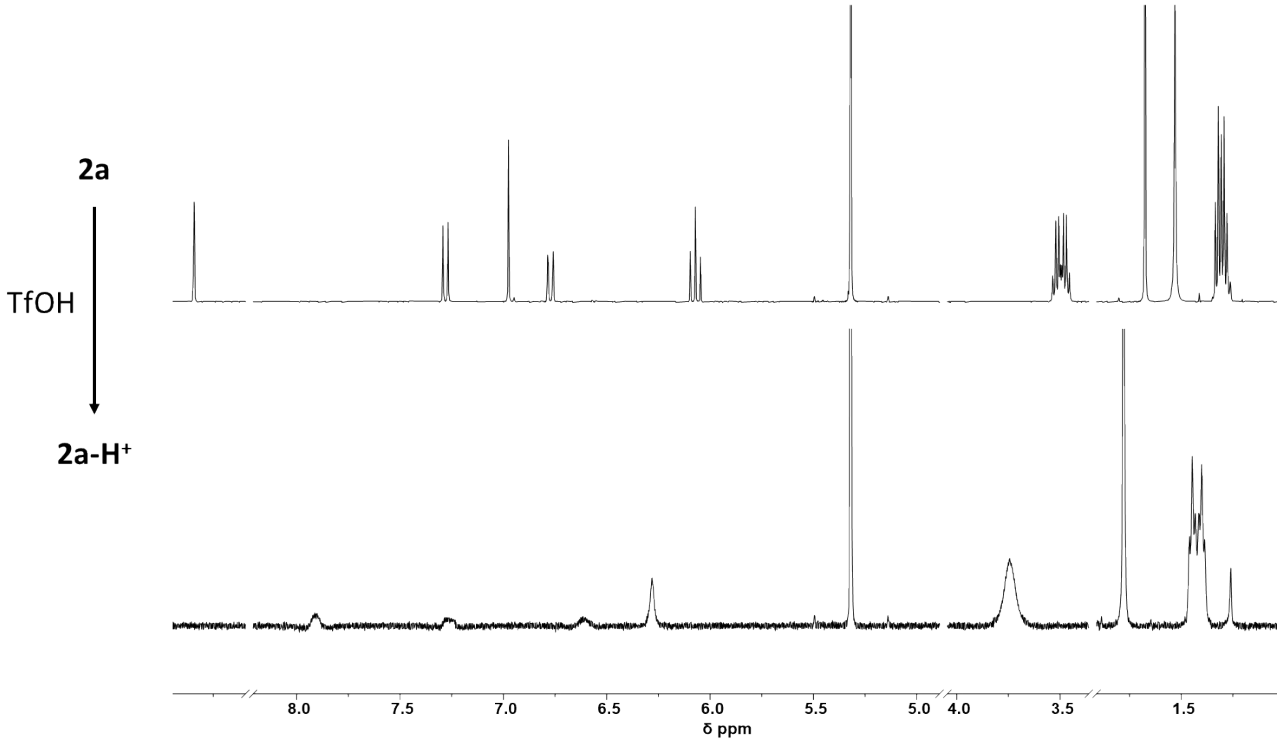

Figure S5: Stacked ^{1}H NMR spectra (500 MHz, CD_2Cl_2, 298 K) of a) DASA **2a** (top), b) the same sample immediately after addition of 1 equivalent of TfOH (bottom). The intensities of the resonances corresponding to the residual solvent (5.32 ppm), and the methyl protons 12 and 13 (1.80 and 1.89 ppm respectively) of **2a** exceed the vertical scale.

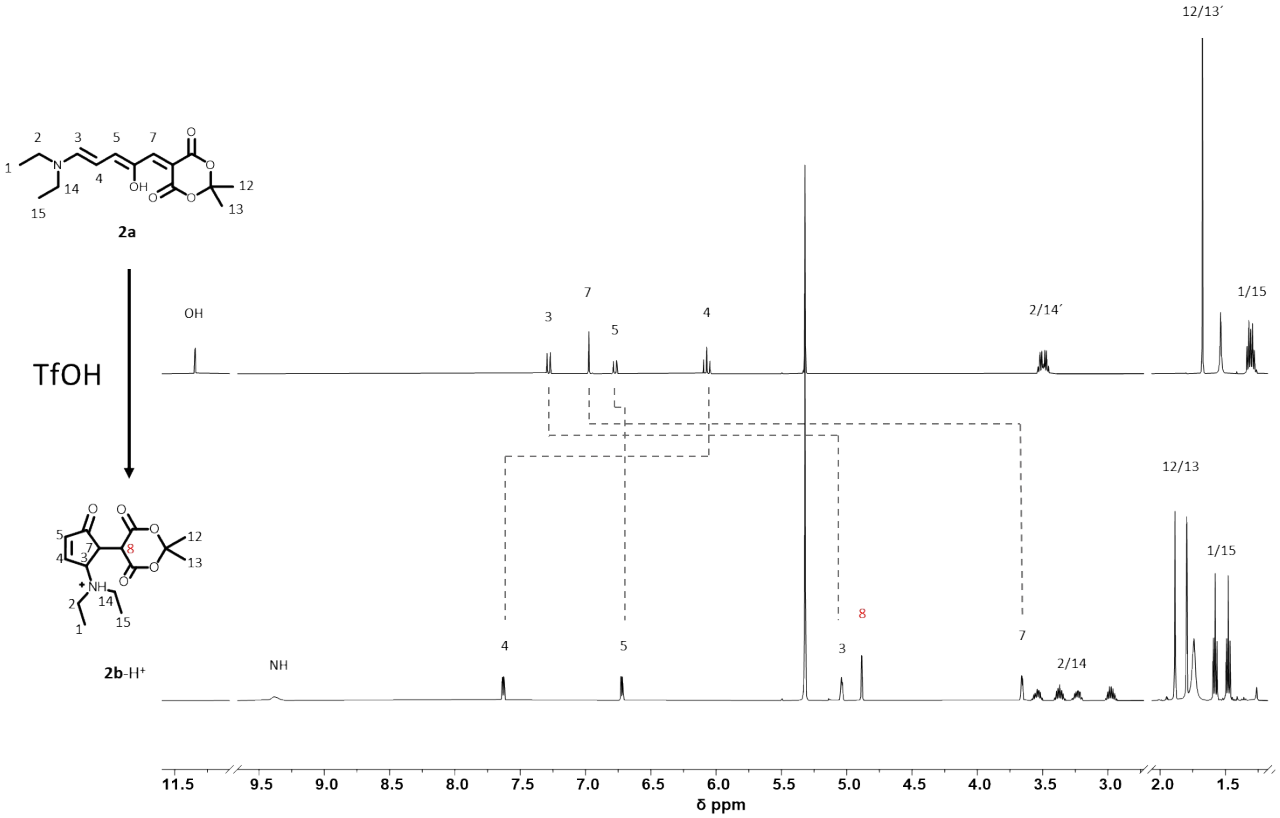

Figure S6: Stacked partial ^{1}H NMR spectra (500 MHz, CD_2Cl_2, 298 K) of a) DASA **2a** (top), b) the same sample after reaction with 1 equivalent of TfOH (bottom).

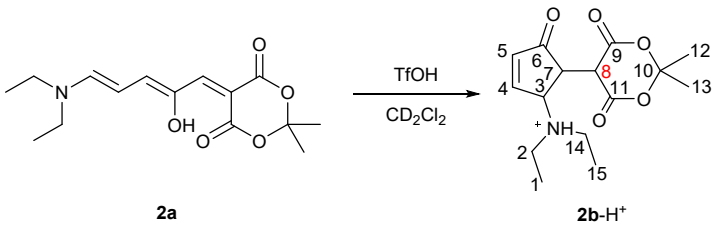

Scheme 3: synthesis of DASA **2b**-H^{+} upon treatment of DASA **2a** with 1 equivalent of TfOH.

^{1}H NMR (500 MHz, CD_2Cl_2, 289 K) δ (ppm) 9.37 (s, 1H, NH), 7.63 (dd, J = 6.1, 2.1 Hz, 1H, H^{4}), 6.72 (dd, J = 6.1, 1.9 Hz, 1H, H^{5}), 5.04 (m, 1H, H^{3}), 4.89 (d, J = 2.0 Hz, 1H, H^{8}), 3.66 (dd, J = 4.2, 2.1 Hz, 1H, H^{7}), 3.60 – 3.49 (m, 1H, H^{2}), 3.44 – 3.32 (m, 1H, H^{2}), 3.23 (dtd, J = 14.8, 7.4, 2.6 Hz, 1H, H^{14}), 2.98 (dp, J = 14.3, 7.2 Hz, 1H, H^{14}), 1.89 (s, 3H, H^{12}), 1.80 (s, 3H, H^{13}), 1.58 (t, J = 7.3 Hz, 3H, H^{1}), 1.48 (t, J = 7.3 Hz, 3H, H^{15}).

^{13}C NMR (126 MHz, CD_2Cl_2, 298 K) δ (ppm) 199.6 (C_6), 165.5 (C_9), 163.9 (C_{11}), 150.8 (C_4), 140.4 (C_5), 107.0 (C_{10}), 66.7 (C_3), 49.9 (C_2), 46.4 (C_{14}), 46.2 (C_7), 45.2 (C_8), 28.4 (C_{12}), 26.5 (C_{13}), 11.2 (C_1), 10.4 (C_{15}).

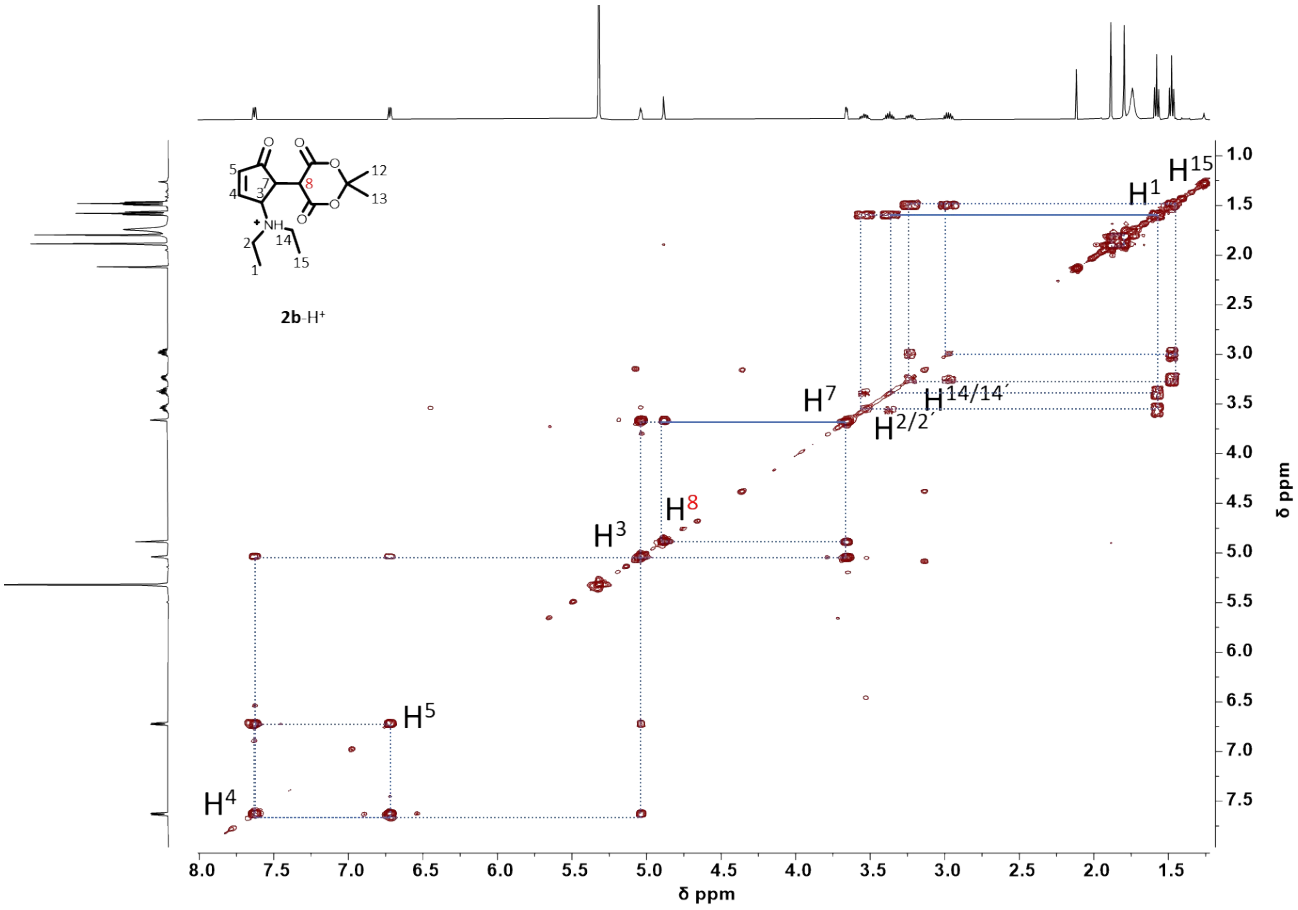

Figure S7: partial COSY spectra of DASA **2b**-H$^+$. (500 MHz, CD_2Cl_2, 298 K). Cross-peaks correlating characteristic signals are highlighted with dashed squares.

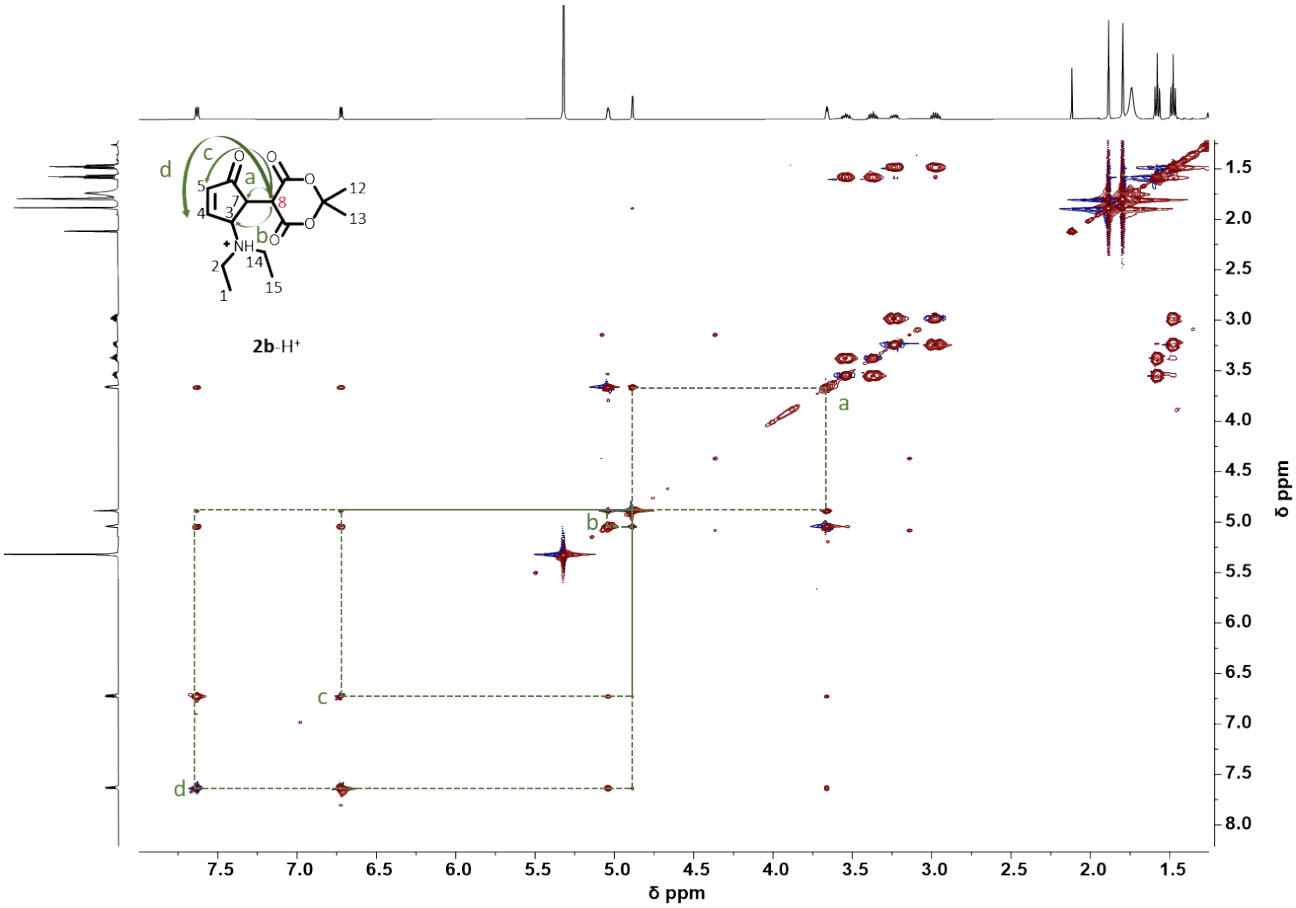

Figure S8: partial TOCSY spectra of DASA **2b**-H$^+$. (500 MHz, CD_2Cl_2, 298 K, spinlock 80 ms). Cross-peaks correlating characteristic signals are highlighted with dashed squares.

Reversibility experiments with a phosphazene base (P_1-t-Bu 0.1 M in deuterated dichloromethane) were carried out as follows: to an NMR tube containing cyclized DASA in deuterated dichloromethane, 1 equivalent of P_1-t-Bu 0.1 M was added. . Upon addition of the base the orange solution rapidly changes to purple which is indicative of formation of the open DASA form. The progress of the reaction was monitored by ^{1}H NMR. The NMR spectra of the final products are consistent with the DASA starting materials **1a** or **2a**.

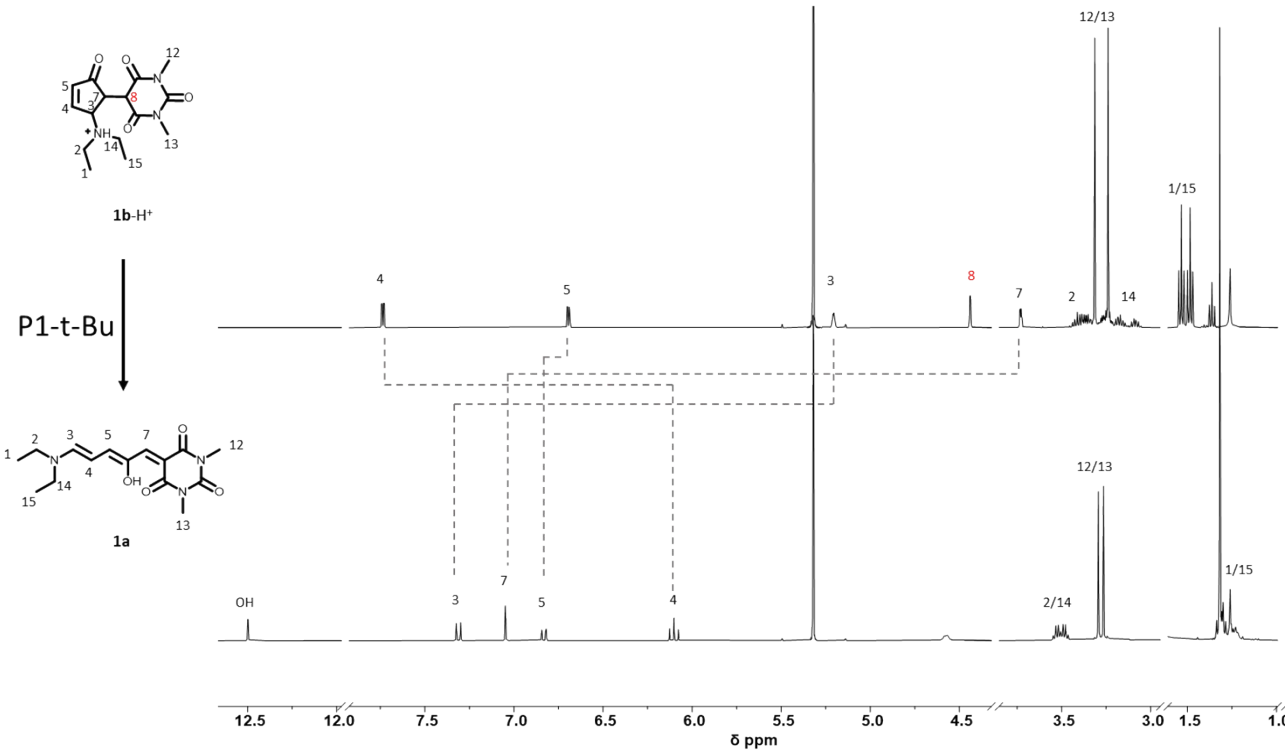

Figure S9: Stacked partial ^{1}H NMR spectra (500 MHz, CD_2Cl_2, 298 K) of a) DASA **1b**-H$^+$ (top), b) the same sample after reaction with 1 equivalent of P1-t-Bu base (bottom).

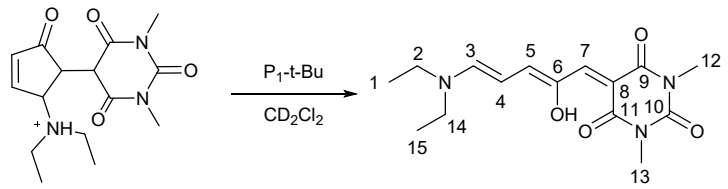

Scheme 4: synthesis of DASA **1a** upon treatment of DASA **1b**-H$^+$ with 1 equivalent of P_1-t-Bu base.

^{1}H NMR (500 MHz, CD_2Cl_2, 298 K) *δ (ppm)* 12.50 (dd, *J* = 1.4, 0.7 Hz, 1H, OH), 7.31 (d, *J* = 12.3 Hz, 1H, H^3), 7.05 (s, 1H, H^7), 6.83 (dd, *J* = 12.5, 0.9 Hz, 1H, H^5), 6.10 (t, *J* = 12.3 Hz, 1H, H^4), 3.57 – 3.45 (m, 4H, $H^{2/14}$), 3.29 (s, 3H, H^{12}), 3.26 (s, 3H, H^{13}), 1.29 – 1.20 (m, 6H, $H^{1/15}$).

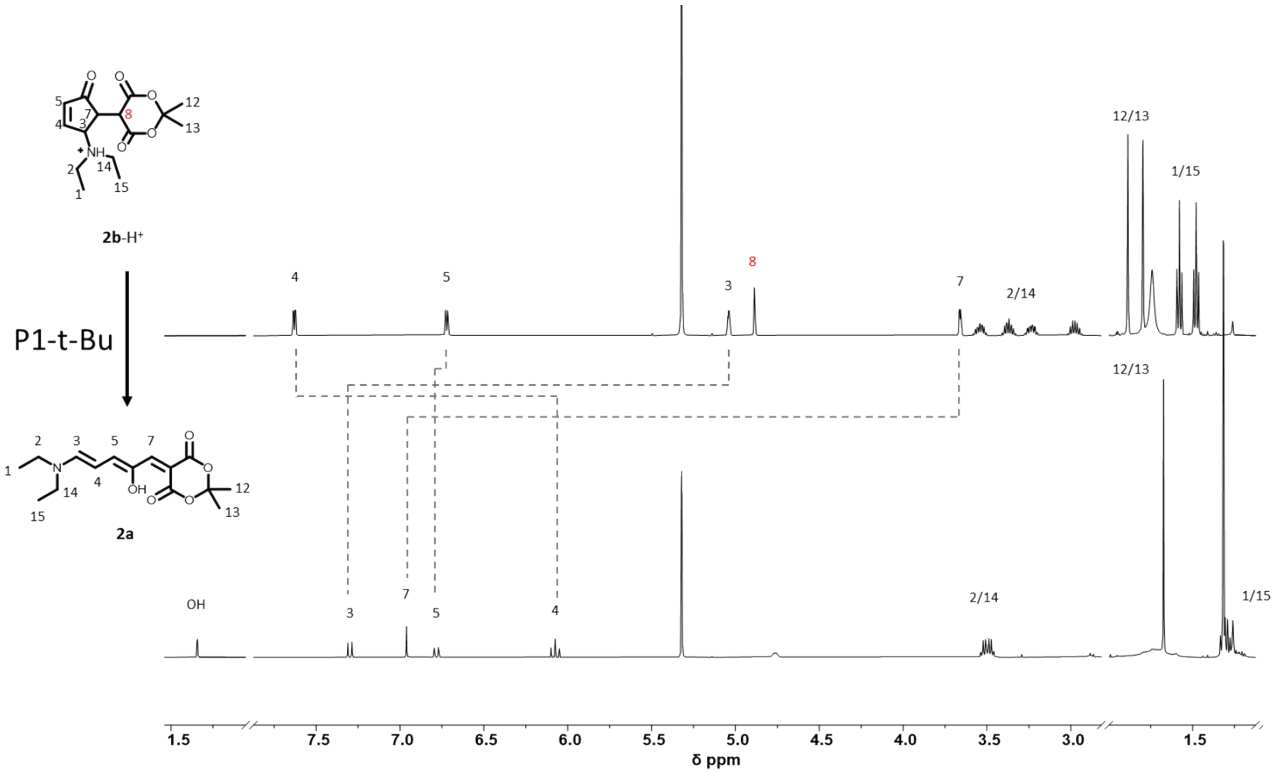

Figure S10: Stacked partial ^{1}H NMR spectra (500 MHz, CD_2Cl_2, 298 K) of a) DASA **2b**-H$^+$ (top), b) the same sample after reaction with 1 equivalent of P1-t-Bu base (bottom).

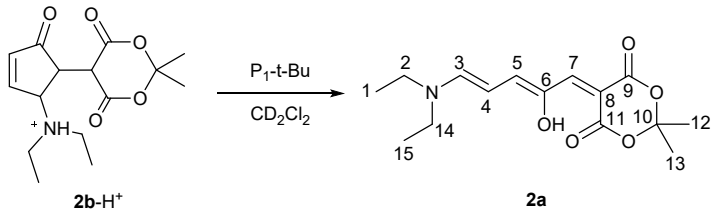

Scheme 5: synthesis of DASA **2a** upon treatment of DASA **2b**-H$^+$ with 1 equivalent of P_1-t-Bu base.

^{1}H NMR (500 MHz, CD_2Cl_2, 289 K) *δ (ppm)* 11.34 (d, J = 0.9 Hz, 1H, OH), 7.30 (d, J = 12.2 Hz, 1H, H^3), 6.96 (s, 1H, H^7), 6.78 (dd, J = 12.7, 1.8 Hz, 1H, H^5), 6.07 (t, J = 12.3 Hz, 1H, H^4), 3.55 – 3.44 (m, 4H, $H^{2/14}$), 1.67 (s, 6H, $H^{12/13}$), 1.31 – 1.23 (m, 6H, $H^{1/15}$).

In order to provide evidence that compound **1b**-H+ was the protonated cyclized DASA **1a** we independently generated **1b** dissolving DASA **1a** in CD_3OD (0.6 mL, 1.06 mg for **1a** 6.18 mM) (Figure S11 top). A mixture containing over 90% **1b** was obtained, that was then protonated adding TfOH (1 equiv.). The middle panel of Figure S11 shows a second set of resonances corresponding to a cyclized species which can be identified as the protonated form of **1b**. Volatiles were removed under vacuum and the residue dissolved in CD_2Cl_2. In the NMR spectrum of the resulting solution

resonances that are fully consistent with those of **1b**-H$^+$ generated by direct protonation of **1a** in CD_2Cl_2 can be identified (Figure S11 bottom).

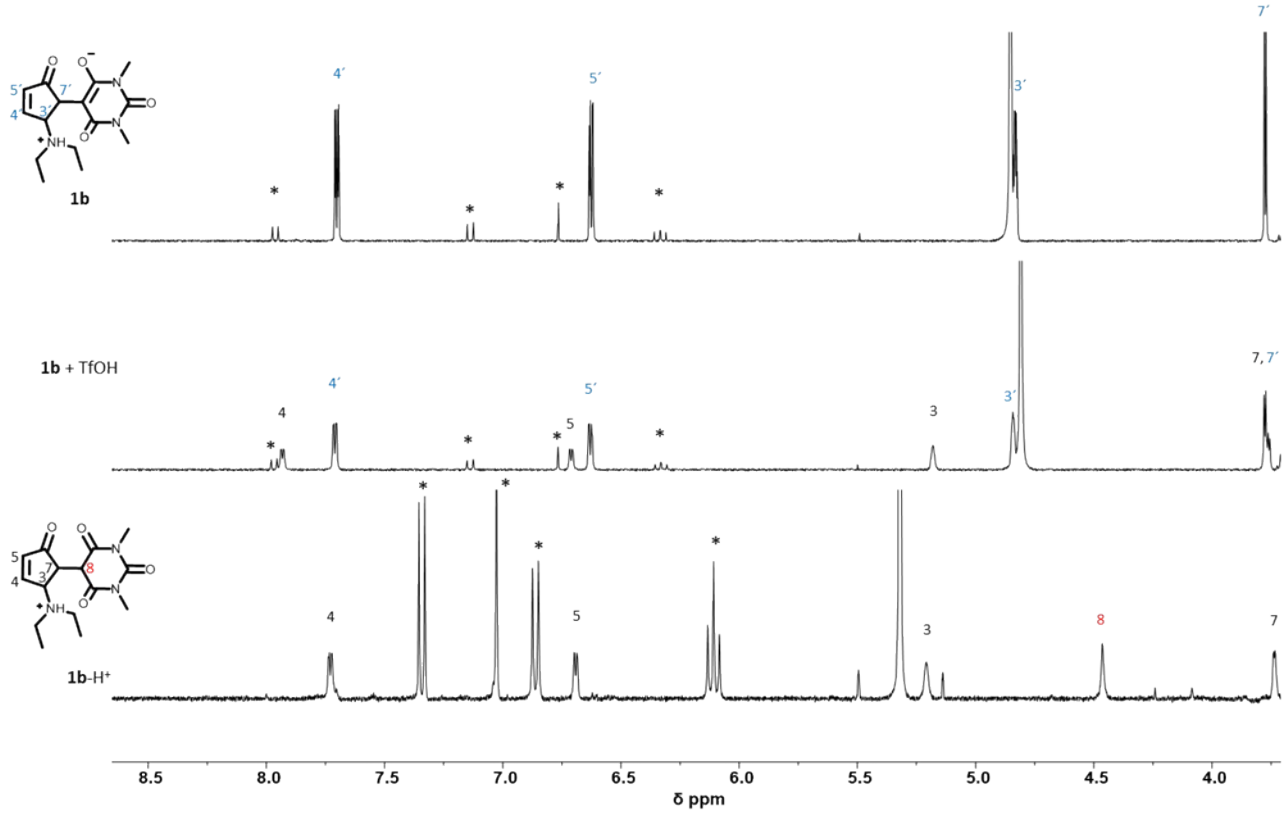

*Figure S11: Stacked partial 1H NMR spectra (500 MHz, 298 K) of **1b** in CD_3OD (top), the same solution upon addition of TfOH (middle) and after concentration and dissolution in CD_2Cl_2 (bottom). Resonances corresponding to **1a** are marked with a (*). Signals corresponding to CD_3OD (4.87 ppm, top and middle panel) and CD_2Cl_2 (5.32 ppm, bottom panel) exceed the vertical scale.*

To try and identify the site at which protonation of open DASA occurs, **1a** (0.5 mL, 0.77 mg 5 mM) was titrated with TfOH in CD_2Cl_2. A stock solution of TfOH (0.1 M) was added in portions to the solution of DASA **1a** (Figure S12). Broadening and shifting is observed for all resonances associated with **1a**. Specifically, protons 1, 3, 7 and 15 exhibited the largest variations in chemical shift. As these signals correspond to protons that are in proximity of both the donor (amine) and the acceptor moieties, no clear trends could be identified. Basing on these results the protonation site cannot be unambiguously assigned.

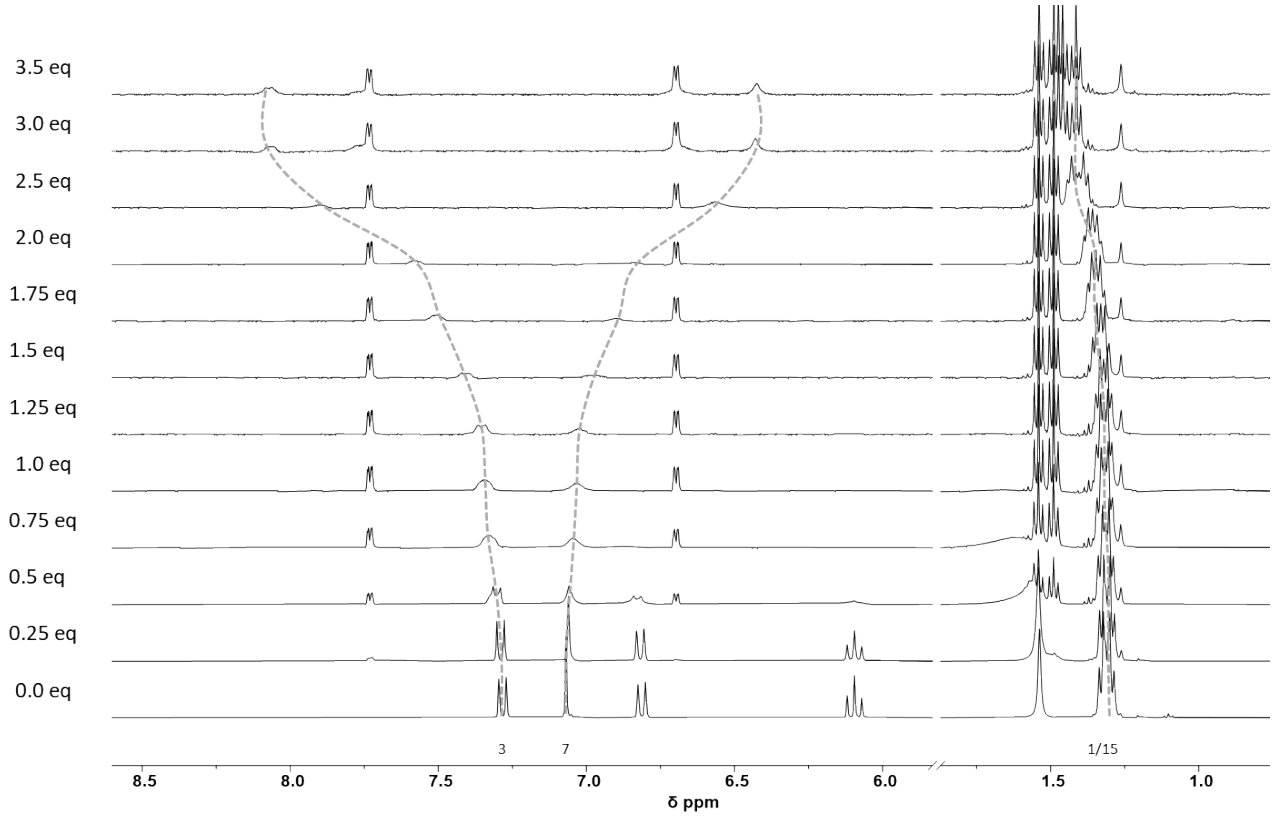

*Figure S12: Stacked partial ^{1}H NMR spectra (500 MHz, CD_2Cl_2, 298 K) of DASA **1a** (5 mM) upon addition of increasing amounts of TfOH (0.1 M).*

4. UV-vis and emission measurements

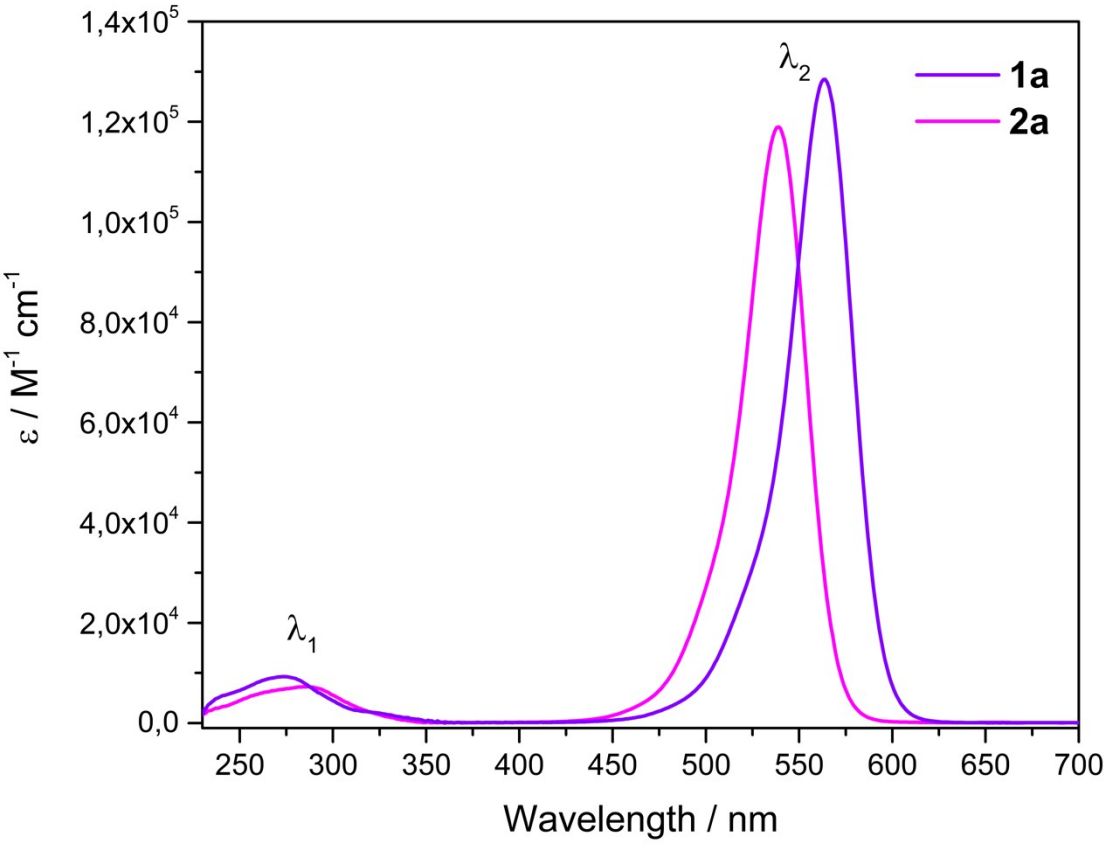

*Figure S13: UV-vis spectra of DASA **1a** and **2a** in dichloromethane.*

	λ_1 (nm) /ε (M^{-1} cm^{-1})	λ_2 (nm)/ε (M^{-1} cm^{-1})
1a	274/9300	564/129000
2a	284/7200	539/118900

Table 1: Absorption maxima and the related absorption coefficients for **1a** and **2a**.

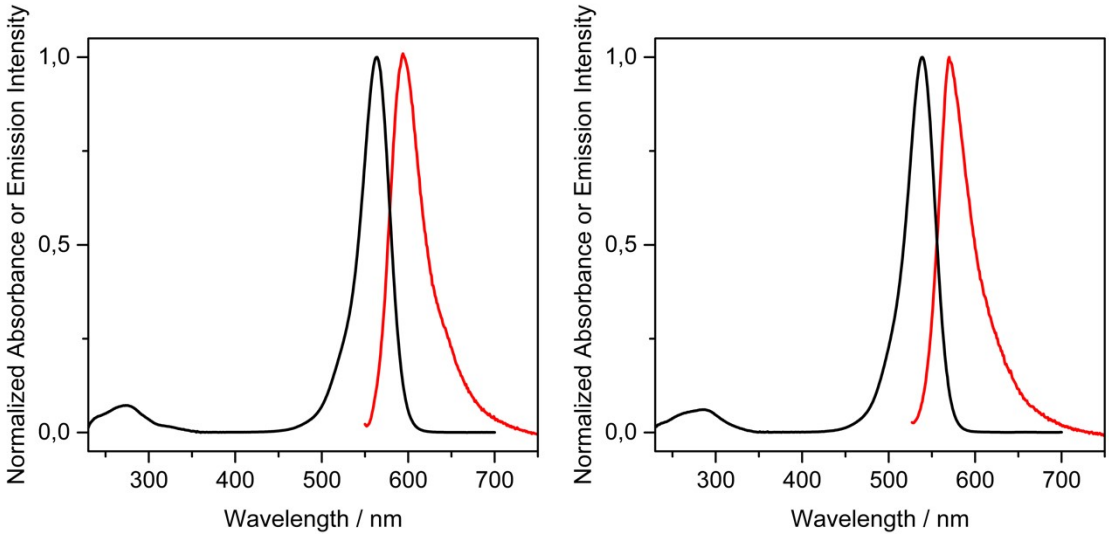

*Figure S14: Normalized UV-vis (black line) and emission (red line) spectra of **1a** (left) and **2a** (right) in dichloromethane.*

	$\lambda_{max,em}$ / nm	Φ_{em}
1a	594	0.10 %
2a	570	0.05 %

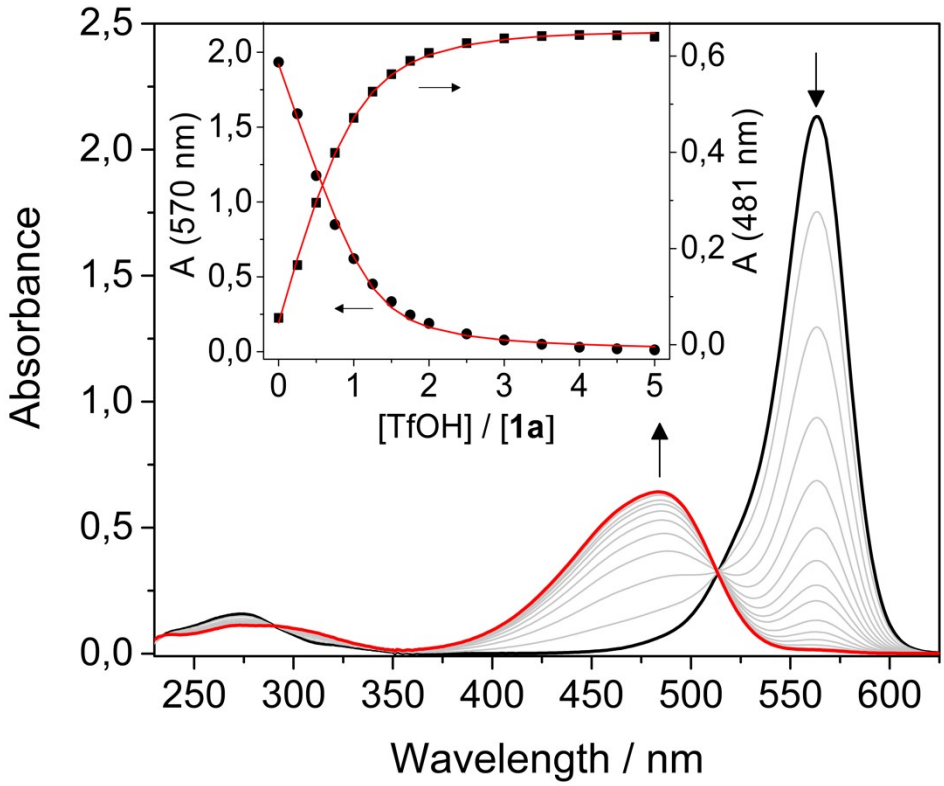

Table 2: Emission maxima and quantum yield of emission for **1a** and **2a**.

Figure S15: Absorption spectra of a 1.6×10^{-5} M solution of **1a** upon addition of increasing amounts of TfOH; the inset shows the absorption changes at 481 nm and 570 nm as a function of acid added, the solid lines are the fitting curves of the experimental data according to a 1:1 binding model.

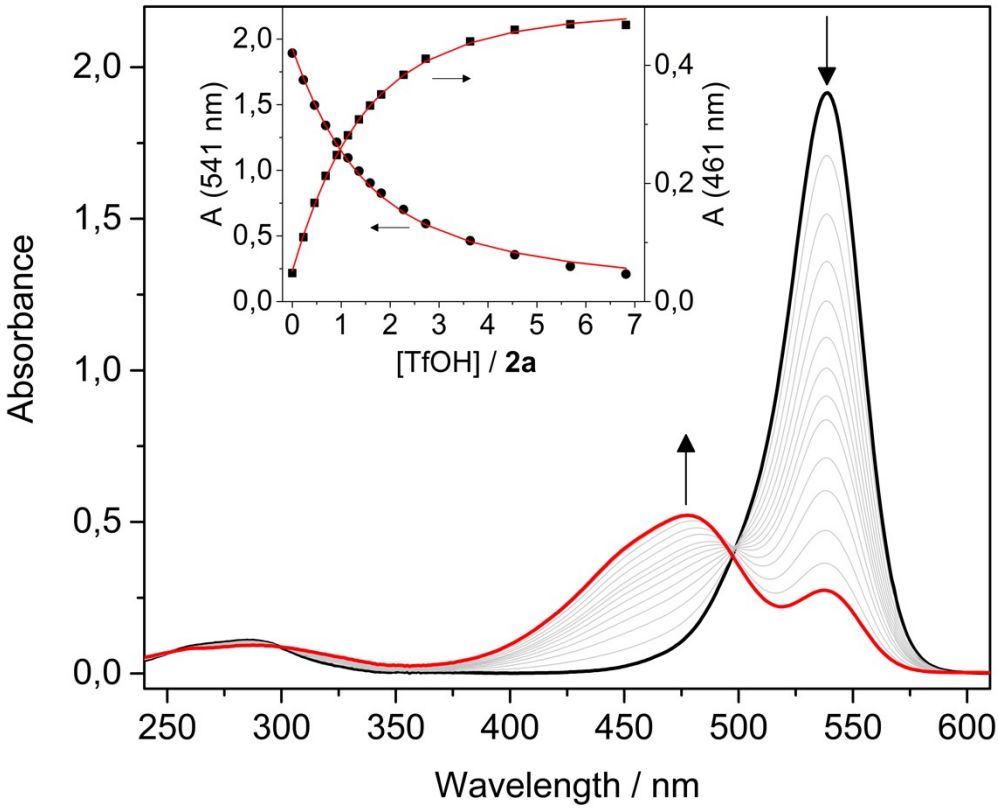

Figure S16: Absorption spectra of a 1.5 × 10^{-5} M solution of **2a** upon addition of increasing amounts of TfOH; the inset shows the absorption changes at 461 nm and 541 nm as a function of acid added, the solid lines are the fitting curves of the experimental data according to a 1:1 binding model.

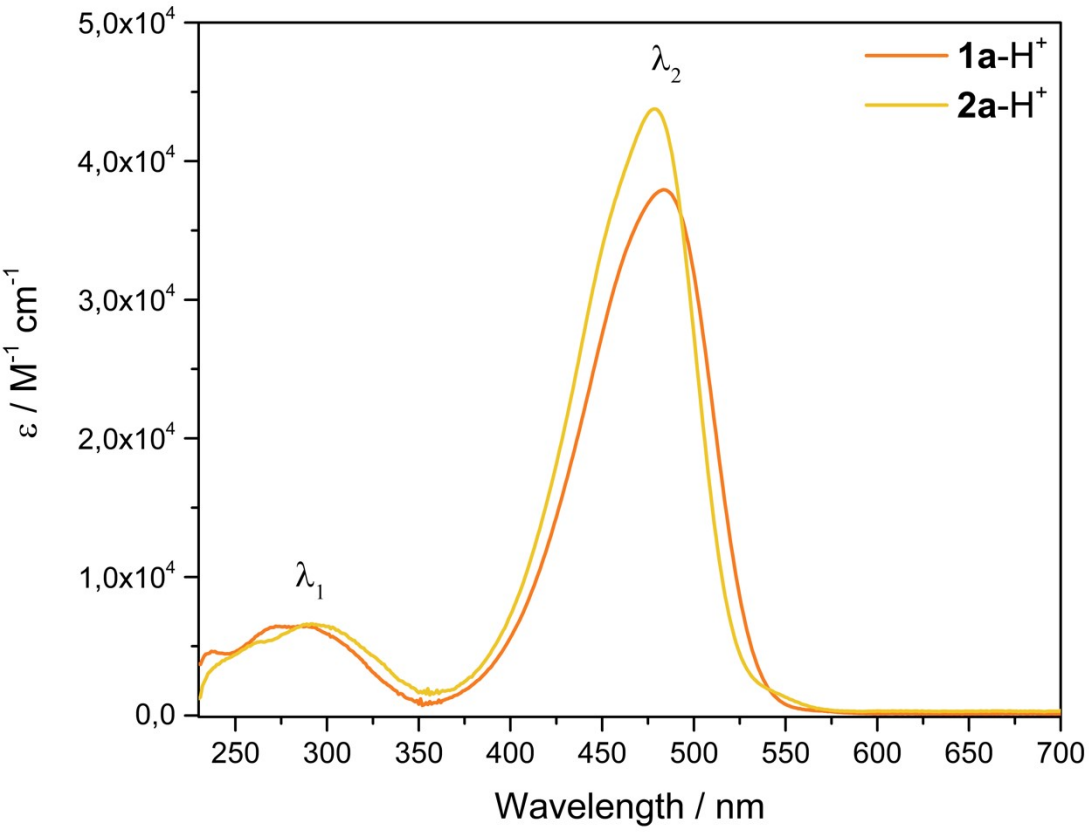

Figure S17: UV-vis spectra of **1a**-H⁺ and **2a**-H⁺ in dichloromethane, obtained by adding excess acid to solutions of known concentrations of **1a** and **2a**.

	λ_1 (nm)/ε (M^{-1} cm^{-1})	λ_2 (nm)/ε (M^{-1} cm^{-1})
1a-H^+	289/6500	484/37900
2a-H^+	291/6600	476/43800

Table 3: Absorption maxima and the related absorption coefficients for **1a**-H^+ and **2a**-H^+.

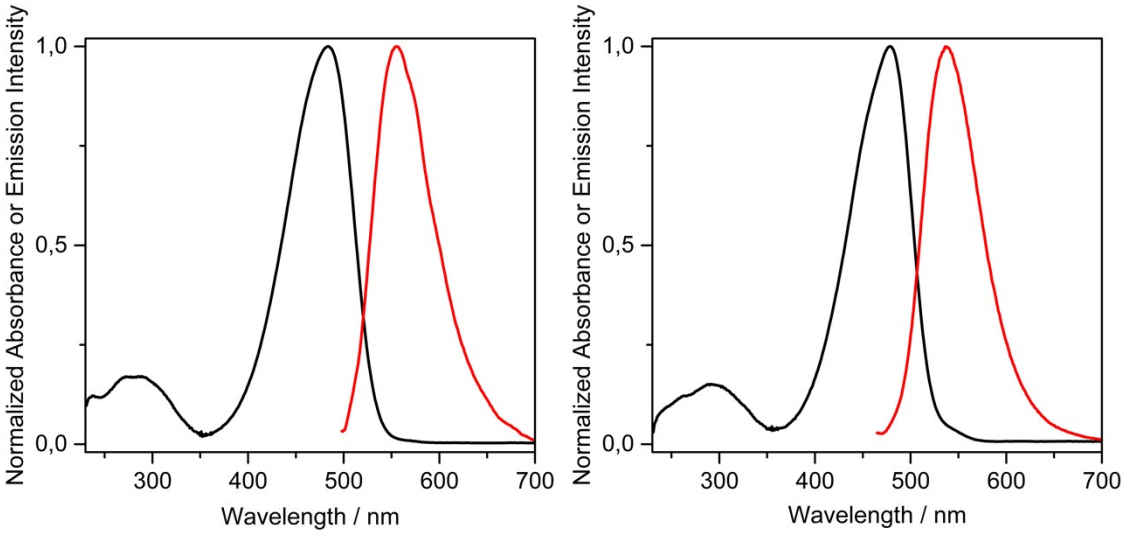

Figure S18: Normalized UV-vis (black line) and emission (red line) spectra of **1a**-H^+ (left) and **2a**-H^+ (right) in dichloromethane.

	$\lambda_{max,em}$ / nm	Φ_{em}
1a-H^+	554	0.14 %
2a-H^+	537	0.10 %

Table 4: Emission maxima and quantum yield of emission for **1a**-H^+ and **2a**-H^+.

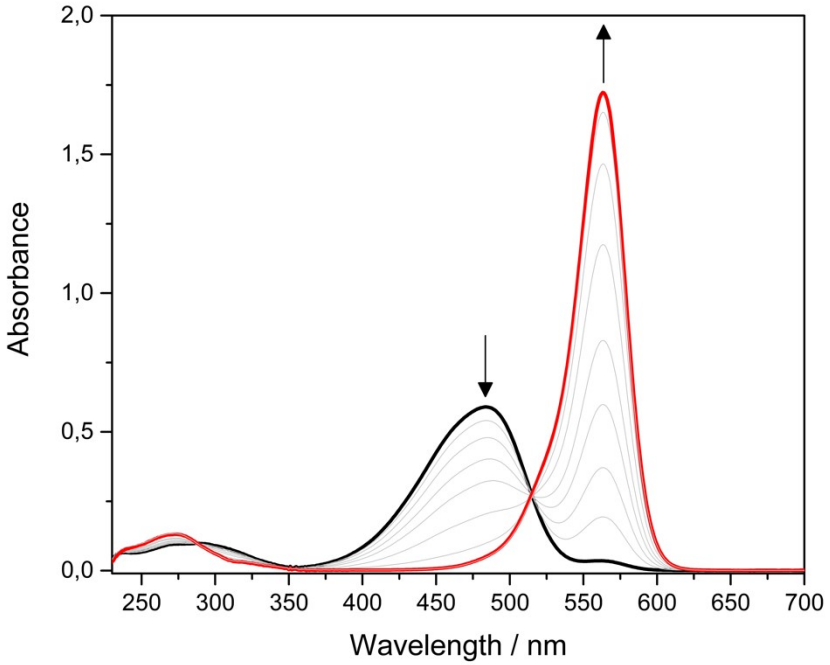

Figure S19: UV-vis experiment showing the reversibility of the open form protonation of **1a**. Direct addition of 2 equivalents of acid to a sample 1.5×10^{-5} M of **1a** afforded the black line. Then, increasing amounts of the phosphazene base P_1 were added up to 2 equivalents, affording the original spectrum of **1a** (red line) with a recovery percentage of 95 % of the initial concentration.

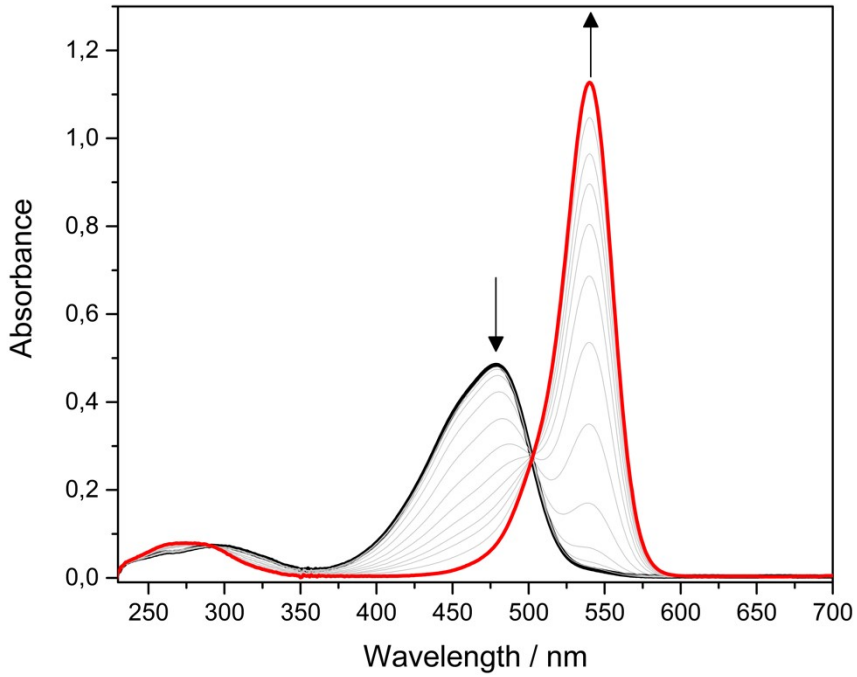

Figure S20: UV-vis experiment showing the reversibility of the open form protonation of **2a**. Direct addition of 7 equivalents of acid to a sample 1.1×10^{-5} M of **2a** afforded the black line. Then, increasing amounts of the phosphazene base P_1 were added up to 7 equivalents, affording the original spectrum of **2a** (red line) with a recovery percentage of 93 % of the initial concentration.

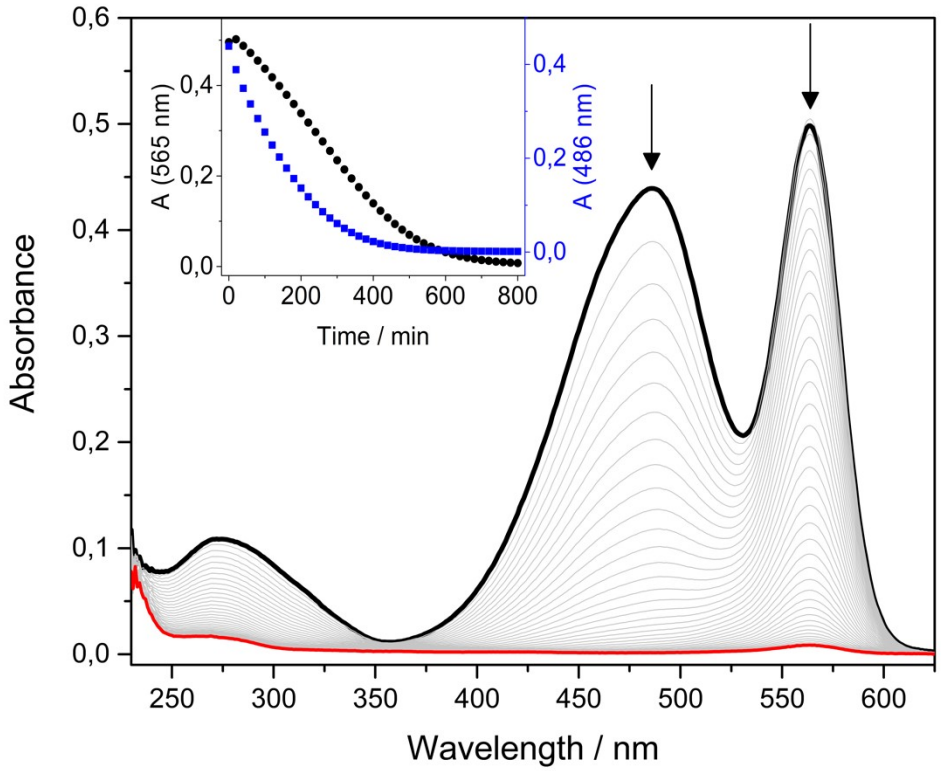

Figure S21: Absorption spectra over time of a 1.5×10^{-5} M solution of **1a** with 1 equivalent of acid added in the dark; the inset shows the absorption changes at 565 nm (black dots) and 486 nm (blue squares) as a function of time. The initial ratio between the two bands reflects the distribution of **1a** and **1a**-H^+ according to the equilibrium constant of the protonation reaction.

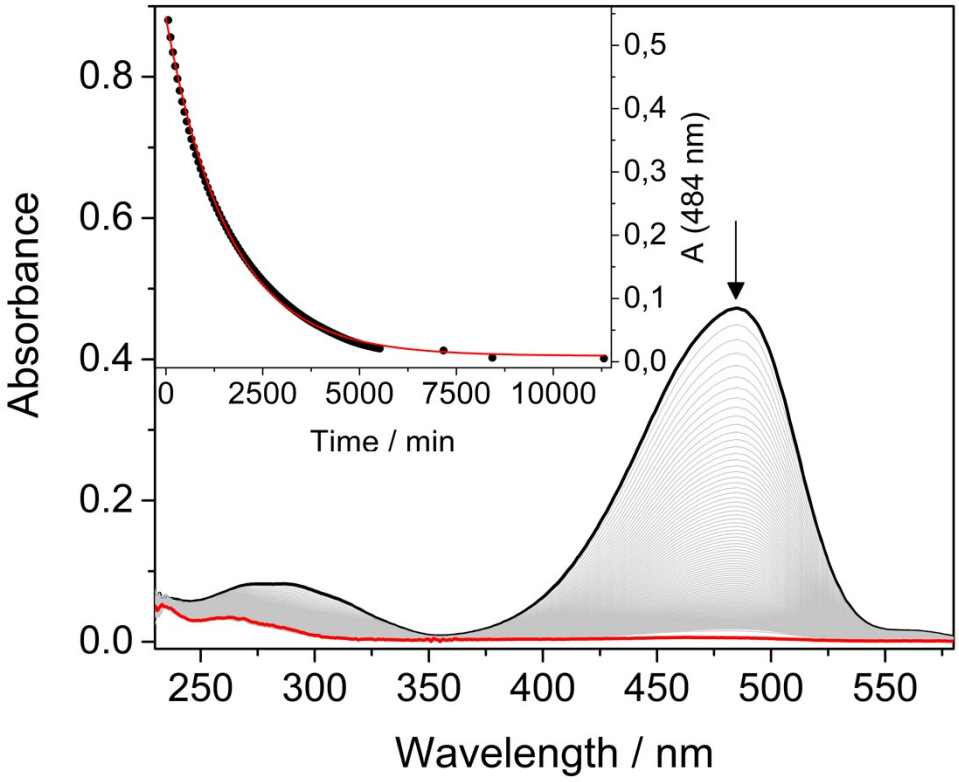

Figure S22: Absorption spectra over time of a 1.5×10^{-5} M solution of **1a** with 3 equivalents of acid added in the dark; the inset shows the absorption changes at 484 nm as a function of time, the solid line is the fitting curve of the experimental data according to a first order model.

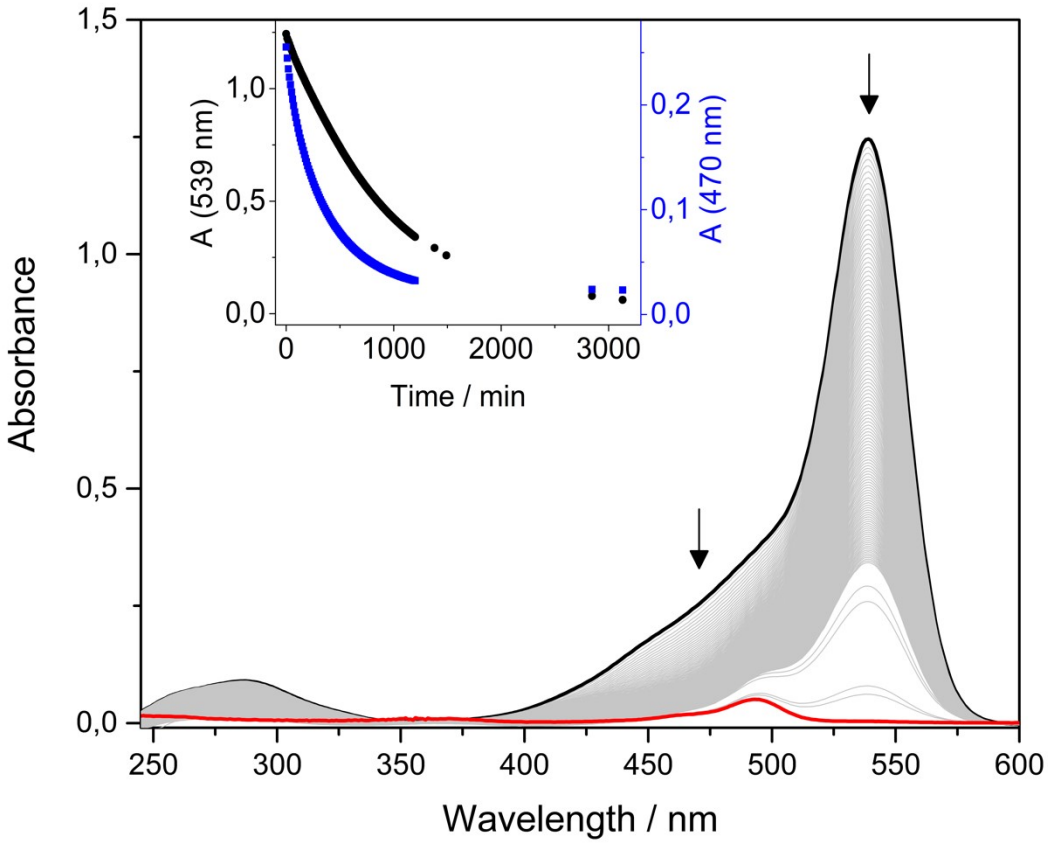

Figure S23: Absorption spectra over time of a 1.5 × 10^{-5} M solution of **2a** with 1 equivalent of acid added in the dark; the inset shows the absorption changes at 539 nm (black dots) and 470 nm (blue squares) as a function of time. The initial ratio between the two bands reflects the distribution of **2a** and **2a**-H^+ according to the equilibrium constant of the protonation reaction.

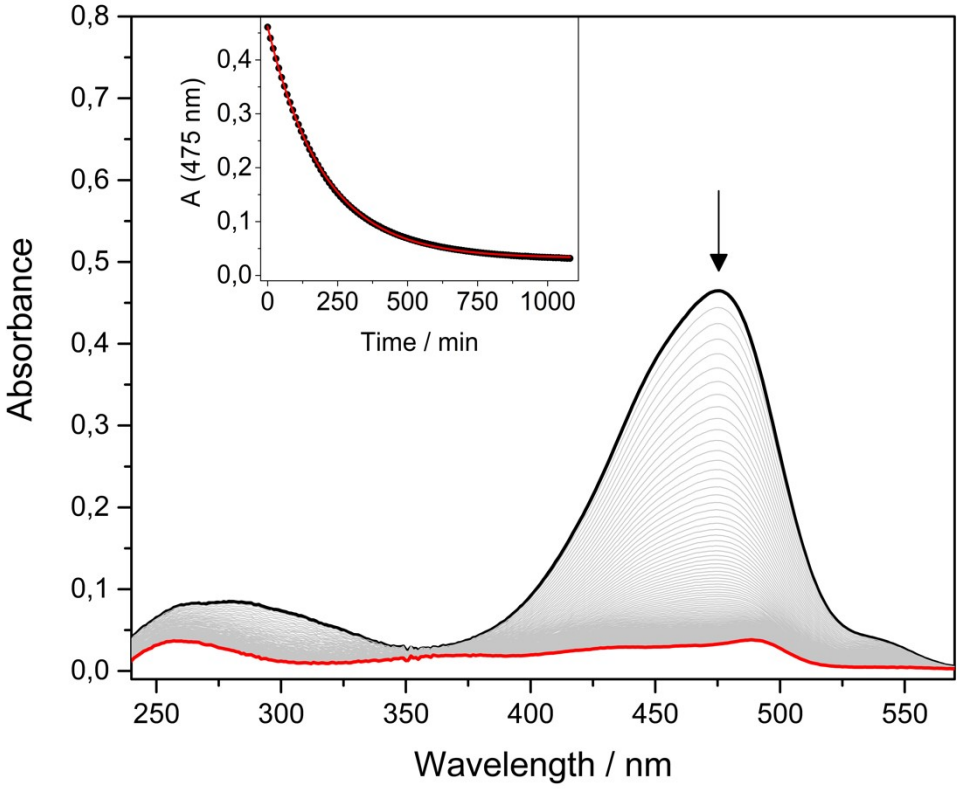

Figure S24: Absorption spectra over time of a 1.5×10^{-5} M solution of **2a** with 10 equivalents of acid added in the dark; the inset shows the absorption changes at 475 nm as a function of time, the solid line is the fitting curve of the experimental data according to a first order model.

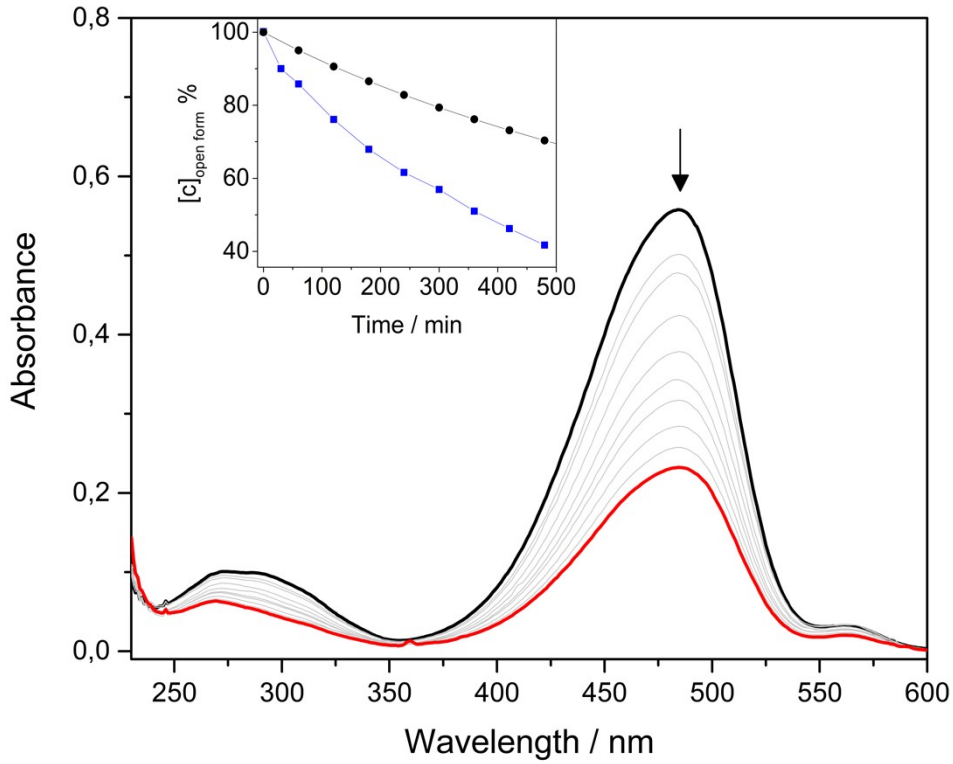

Figure S25: Absorption spectra over 8 h of a 1.5×10^{-5} M solution of **1a** with 3 equivalents of acid added under visible light irradiation; the inset compares the thermal kinetic trace (black dots) with the photokinetic trend (blue squares), obtained by normalizing the absorption variations at the λ_{max}.

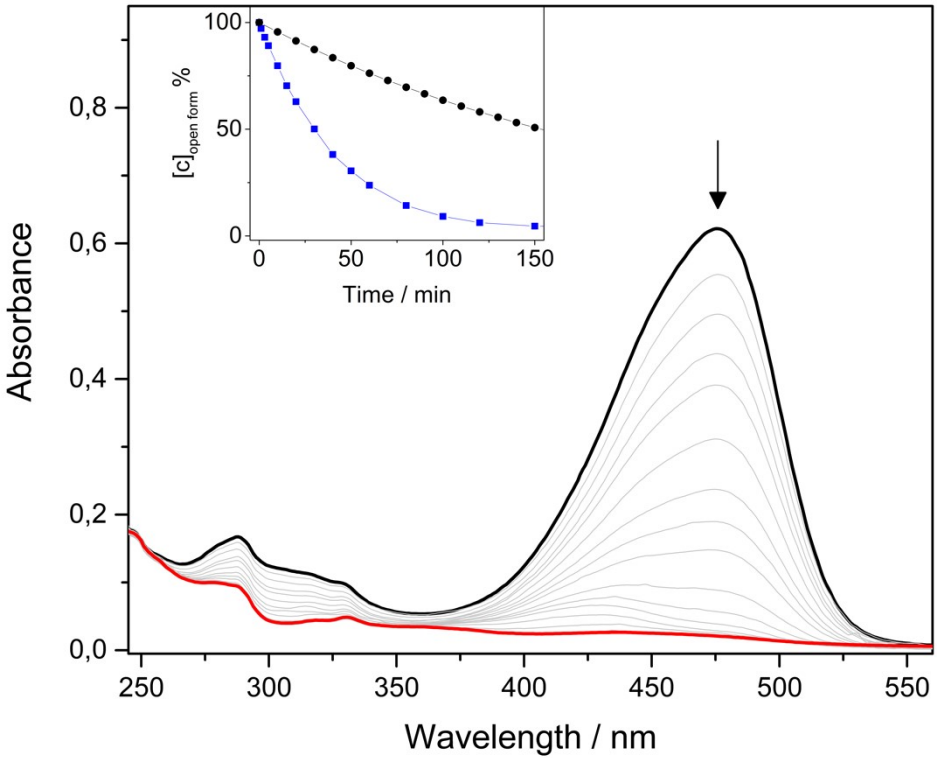

Figure S26: Absorption spectra over 2.5 h of a 1.5×10^{-5} M solution of **2a** with 10 equivalents of acid added under visible light irradiation; the inset compares the thermal kinetic trace (black dots) with the photokinetic trend (blue squares), obtained by normalizing the absorption variations at the λ_{max}.

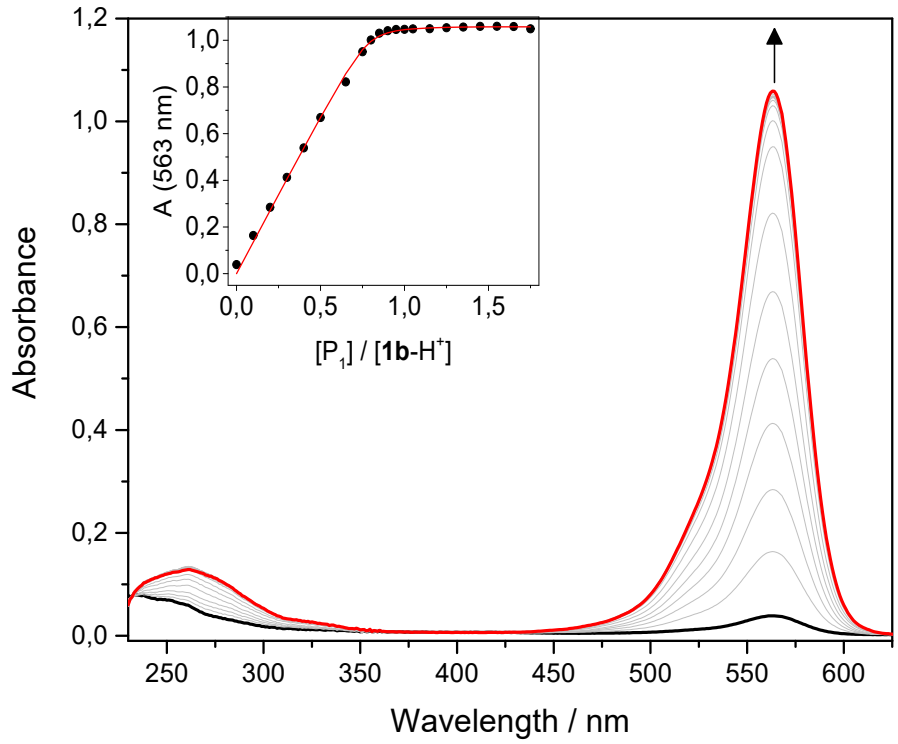

Figure S27: Absorption spectra of a 1.5 × 10^{-5} M solution of **1b**-H^+ upon addition of increasing amounts of P_1; the inset shows the absorption changes at 563 nm as a function of base added, the solid line is the fitting curve of the

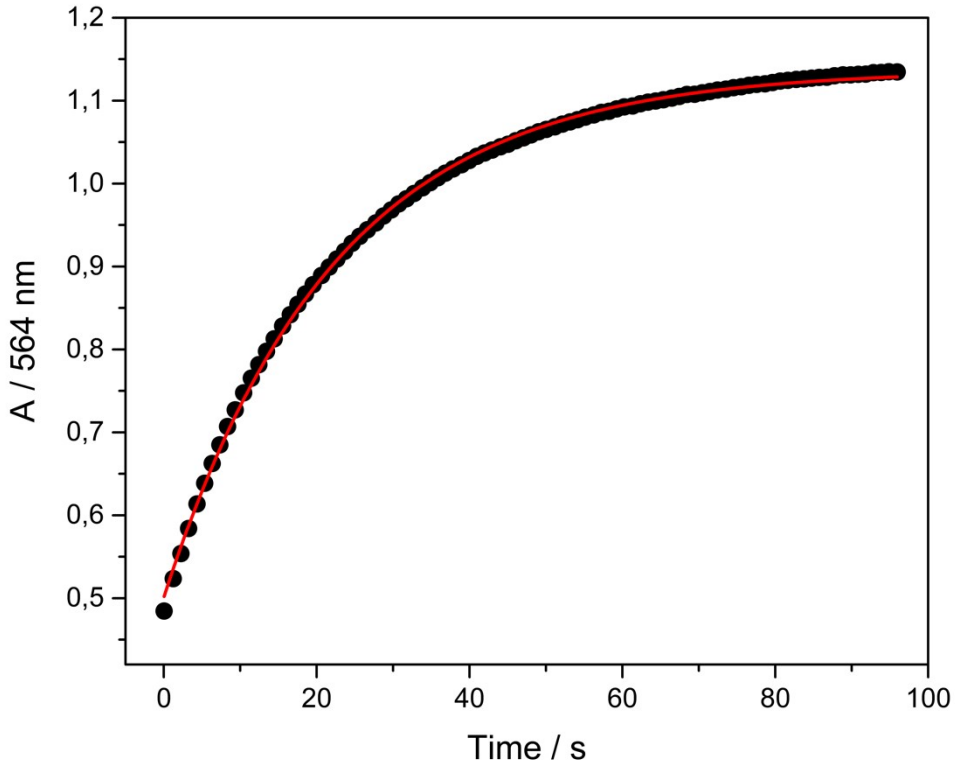

experimental data according to a 1:1 binding model. The recovery percentage of **1a** amounts to 85%.

Figure S28: Absorption changes at 564 nm over time of a 1.0 × 10^{-5} M solution of **1b**-H^+ upon addition of 1 equivalent of P_1; the solid line is the fitting curve of the experimental data according to a first order model.

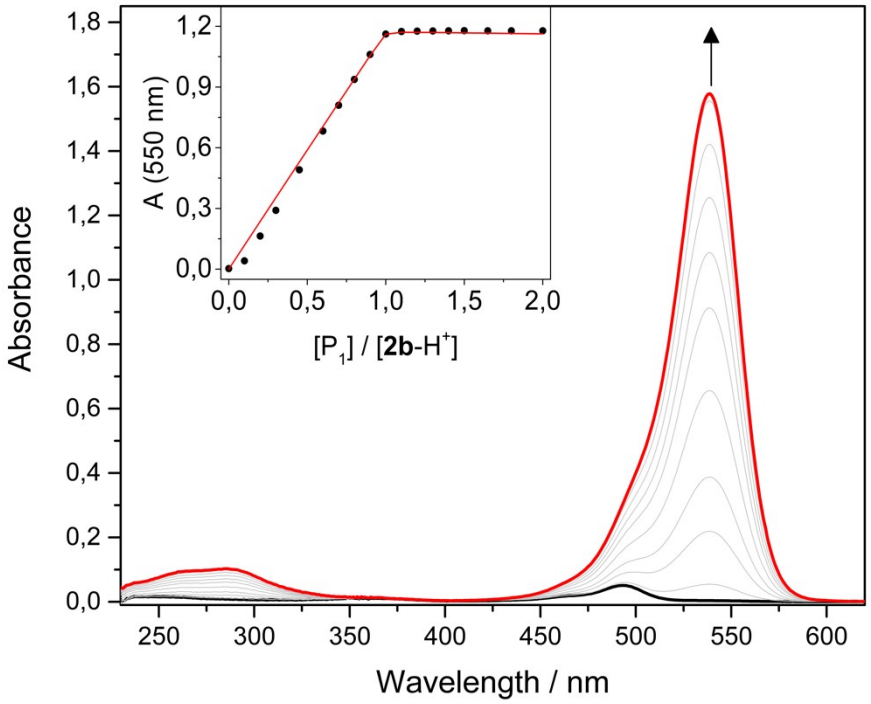

Figure S29: Absorption spectra of a 1.5×10^{-5} M solution of **2b**-H^+ upon addition of increasing amounts of P_1; the inset shows the absorption changes at 550 nm as a function of base added, the solid line is the fitting curve of the experimental data according to a 1:1 binding model. The recovery percentage of **2a** amounts to 89%.

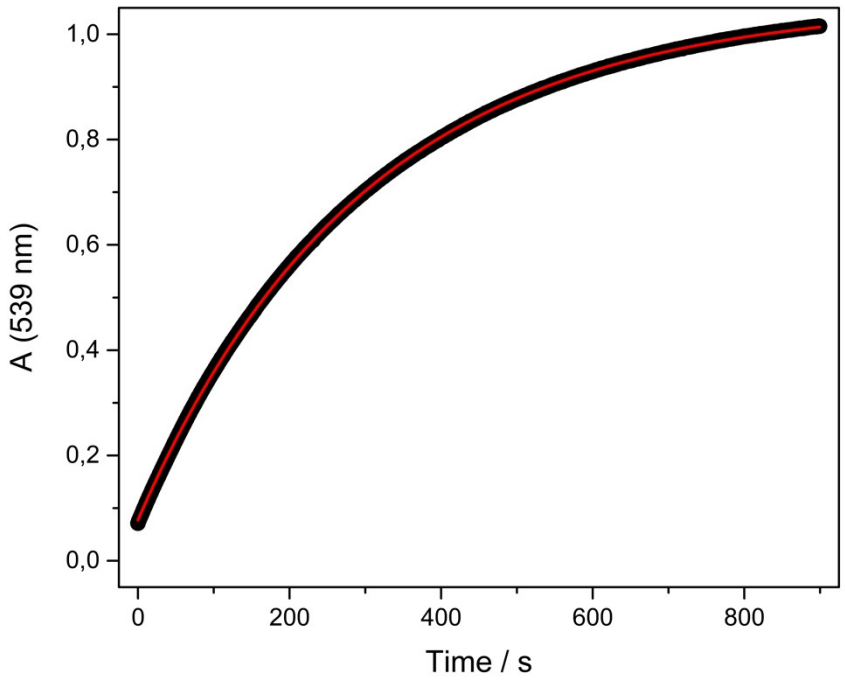

Figure S30: Absorption changes at 539 nm over time of a 1.0×10^{-5} M solution of **2b**-H^+ upon addition of 1 equivalent of P_1; the solid line is the fitting curve of the experimental data according to a first order model.

5. Crystal Structures

Crystals were obtained by vapor diffusion in DCM/diethyl ether (Et_2O) as follows: in a vial 6 mg of compound **1a** were dissolved in minimal amount of DCM. Afterwards one equivalent of trifluoromethanesulfonic acid (TfOH) 0.1 M was added. The vial was inserted in a bigger vial containing Et_2O and the sample was capped and kept in the dark allowing for crystals to grow. The obtained crystals were orange/brown. The same procedure was followed to obtain crystals from the reaction of compound **2a** with TfOH.

Molecular Structure of 1b-H$^+$. The molecular structure of **1b**-H$^+$ is illustrated in Figure S31. It is of cationic nature, due to the tetra-coordinated $[N(7)R_3H]^+$ ammonium atom (N7), that is balanced by the presence of one triflate anion per molecule (omitted in Figure).

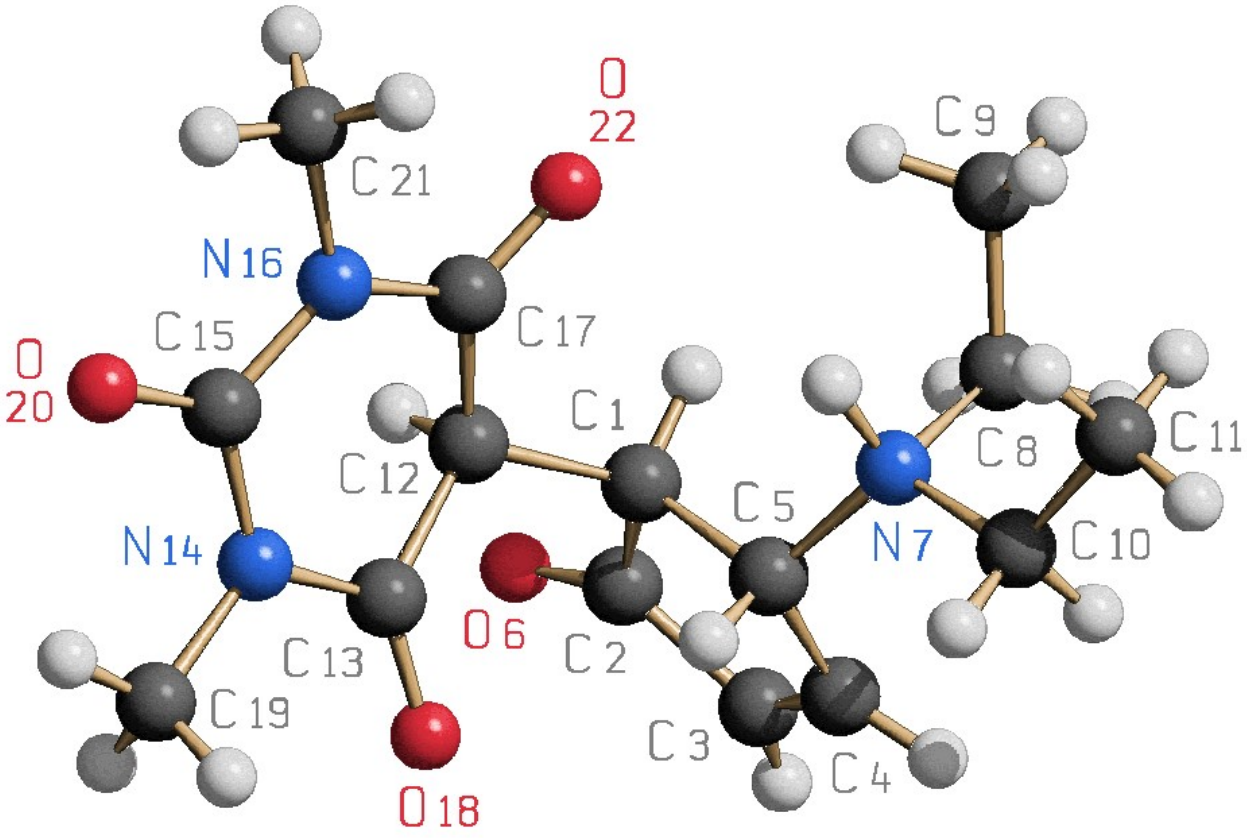

*Figure S31: crystal structure of DASA **1b**-H$^+$. Triflate anion was omitted for clarity.*

The three C=O distances in the six-member ring are comprised between 1.190(15) and 1.199(16) Å (average 1.194 Å), confirming the presence of a double bond between the corresponding C and O

atoms. In fact, single C-O bond distances observed in C-OH or C-O^- groups are significantly longer, more specifically around 1.360-1.375 Å.[9-10]

The tetra-coordination of N7 is not only indirectly confirmed by the presence of the triflate counterion, but also by its tetrahedral geometry, which is substantiated by the angles N7 describes with its substituents. In fact, they vary from 105° (2) with the ethyl groups, to 117.4° (16) and 111.1° (1) (average 114.3°) with the bulkier 5-member ring.

The solid-state packing shows an ionic arrangement, being the triflate anions surrounded by the cationic organic units, and it is also driven by some intermolecular hydrogen bonds, albeit with different strengths. The stronger contacts are found between some of the oxygen atoms in the triflate anion and the nitrogen atom of the ammonium centre and that of the six-member rings, with an average O---N distance of 2.897 Å. Additional significant hydrogen bonds can be identified between a fluorine atom of the triflate anion and one of the methyl substituents of the six-member ring, with a F---C distance of 3.028(37) Å.

Molecular structure of 2b-H^+. The molecular structure of cyclized DASA **2b**-H^+ is illustrated in Figure S32.

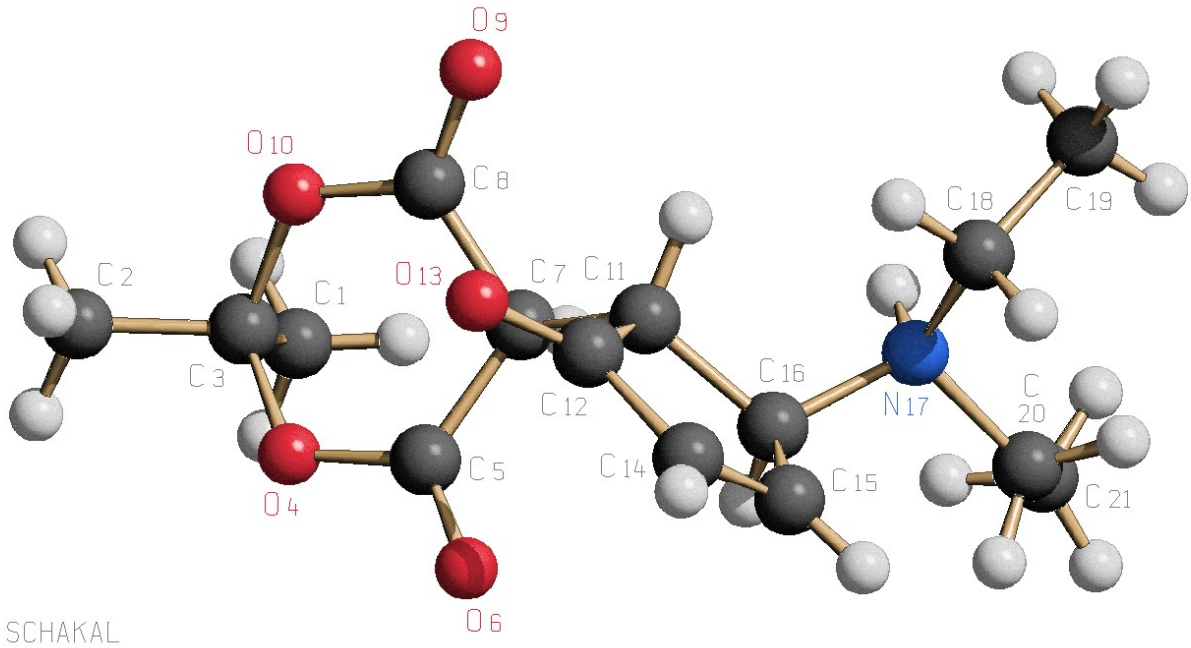

*Figure S32: crystal structure of DASA **2b**-H^+.*

Similarly to previous observations for compound **1b**-H^+, the cationic nature of **2b**-H^+ is confirmed by the presence of one triflate anion (omitted in Figure), and it is due to the tetra-coordination of the unique nitrogen atom. The tetrahedral disposition is confirmed by the value of the angles of the N substituents, with an average value of 111.5°. The two C=O distances in the six-member ring confirm the presence of a double bond between the involved atoms, their average value being equal to 1.195 Å. The same applies for the unique C=O bond in the five-member ring, whose lengths measures 1.201(0) Å.

The solid-state packing is comparable to compound **1b**-H^+, that is each triflate anion is surrounded by the cationic molecules. The most significant hydrogen bond is the one present between one oxygen atom within the triflate ion and the nitrogen atom, with a N---O distance of 2.792 Å.

Crystallographic data for compounds **1b**-H^+ and **2b**-H^+ are reported in Table 5.

Compound	**1b**-H^+	**2b**-H^+
Formula	$C_{16}H_{22}F_3N_3O_7S$	$C_{16}H_{22}F_3NO_8S$
Fw	457.42	445.40
Crystal system	Orthorhombic	Monoclinic
Space group	$P2_12_12_1$	$P2_1/c$
a (Å)	10.2011(18)	8.9554(8)
b (Å)	12.202(2)	21.609(2)
c (Å) Orthorhombic	16.775(3)	10.7441(11)
α (deg)	90	90
β (deg)	90	101.285(3)
γ (deg)	90	90
Cell volume (Å^3)	2088.0(7)	2039.0(4)
Z	4	4
D (g/cm^3)	1.455	1.451
μ (mm^{-1})	0.224	0.228
F(000)	952	928

θ limits (deg)	2.064 to 24.999	2.150 to 24.994
Index ranges	-12<=h<=12, -14<=k<=14, -19<=l<=19	-10<=h<=10, -25<=k<=25, -12<=l<=12
Reflections collected	18010	23362
Independent reflections	3611 [R(int) = 0.1202]	3398 [R(int) = 0.0701]
Completeness to θ max	99.0%	94.6%
Data/restraints/parameters	3611 / 280 / 364	3398 / 0 / 266
Goodness of fit	1.214	1.231
R_1 (I > 2σ(I))	0.1399	0.0915
wR_2 (all data)	0.3109	0.1906
Largest diff. peak and hole, e $Å^{-3}$	0.637 and -0.348	0.411 and -0.384

Table 5: Crystallographic data for compounds **1b**-H^+ and **2b**-H^+ (for labels refer to Figure S31 and S32).

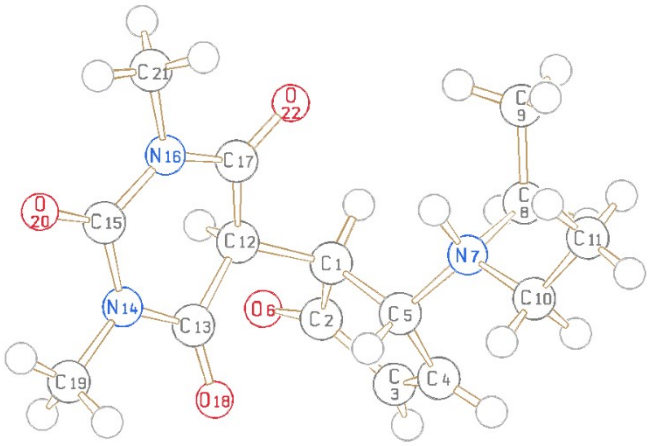

*Figure S33: Molecular structure of **1b**-H⁺ with labelled atoms.*

C(1)-C(2)	1.512(18)
C(1)-C(5)	1.527(18)
C(1)-C(12)	1.560(16)
C(2)-O(6)	1.223(17)
C(2)-C(3)	1.46(2)
C(3)-C(4)	1.29(2)
C(4)-C(5)	1.498(18)
C(5)-N(7)	1.492(16)
N(7)-C(10)	1.47(3)
N(7)-C(100)	1.53(5)
N(7)-C(80)	1.55(5)
N(7)-C(8)	1.56(3)
C(8)-C(9)	1.49(3)
C(10)-C(11)	1.49(3)
C(80)-C(90)	1.50(5)
C(100)-C(110)	1.53(5)
C(12)-C(17)	1.479(18)
C(12)-C(13)	1.525(18)
C(13)-O(18)	1.192(15)
C(13)-N(14)	1.369(16)
N(14)-C(15)	1.410(18)
N(14)-C(19)	1.464(19)
C(15)-O(20)	1.199(16)
C(15)-N(16)	1.385(18)
N(16)-C(17)	1.365(16)
N(16)-C(21)	1.480(18)
C(17)-O(22)	1.190(15)
S(100)-O(102)	1.31(2)
S(100)-O(101)	1.33(3)
S(100)-O(111)	1.38(3)
S(100)-O(113)	1.41(4)
S(100)-O(112)	1.56(3)
S(100)-O(103)	1.60(3)
S(100)-C(104)	1.74(3)
C(104)-F(115)	1.24(4)
C(104)-F(107)	1.30(4)
C(104)-F(116)	1.35(4)
C(104)-F(105)	1.36(4)
C(104)-F(106)	1.47(4)
C(104)-F(117)	1.53(4)

Table 6: Bond distances for Compound **1b-H⁺** (for labels refer to Figure S31).

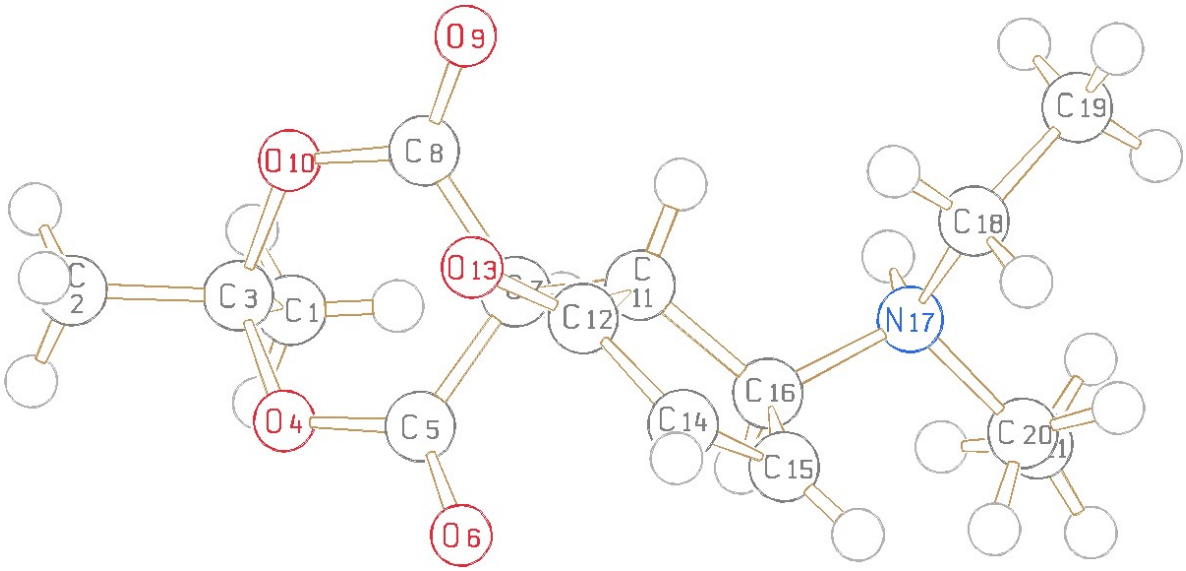

Figure S34: Molecular structure of **2b**-H^+ with labelled atoms.

Table 7: Bond distances for Compound **2b**-H^+ (for labels refer to Figure S32).

C(1)-C(3)	1.491(8)
C(2)-C(3)	1.505(8)
C(3)-O(10)	1.439(6)
C(3)-O(4)	1.439(7)
O(4)-C(5)	1.326(6)
C(5)-O(6)	1.199(6)
C(5)-C(7)	1.502(7)
C(7)-C(8)	1.519(6)
C(7)-C(11)	1.524(6)
C(8)-O(9)	1.191(5)
C(8)-O(10)	1.331(6)
C(11)-C(16)	1.527(7)
C(11)-C(12)	1.533(7)
C(12)-O(13)	1.201(7)
C(12)-C(14)	1.446(9)
C(14)-C(15)	1.306(9)
C(15)-C(16)	1.505(8)
C(16)-N(17)	1.508(7)
N(17)-C(18)	1.511(6)
N(17)-C(20)	1.514(7)
C(18)-C(19)	1.496(8)
C(20)-C(21)	1.430(9)
S(20)-O(21)	1.407(5)
S(20)-O(23)	1.413(4)
S(20)-O(22)	1.421(4)
S(20)-C(24)	1.813(7)
C(24)-F(25)	1.288(7)
C(24)-F(27)	1.299(7)
C(24)-F(26)	1.311(8)

6. Numerical simulations

	1a	**2a**
k_1 (M^{-1} s^{-1})[a]	5.0×10^4	6.3×10^4
k_{-1} (s^{-1})[a]	0.1	1.0
k_2 (s^{-1})[b]	1.0×10^{-5}	8.0×10^{-5}
k_{-2} (s^{-1})[c]	1.0×10^{-8}	8.0×10^{-8}
k_3 (s^{-1})[d]	4.5×10^{-5}	3.3×10^{-6}

The kinetic behavior of the reaction network was simulated taking into consideration all the reactions shown in scheme 5. To compare the experimental data with the simulated concentration profiles, absorbances were converted to concentrations using the absorption coefficients of each species. During all simulations, the initial concentrations of **1a** and **2a** were set to 1.5×10^{-5} M. For compound **1a**, it was simulated the concentration profile in presence of 1 equivalent ($[H^+] = 1.5 \times 10^{-5}$ M) and 3 equivalents ($[H^+] = 4.5 \times 10^{-5}$ M) of acid. For compound **2a**, it was simulated the concentration profile in presence of 1 equivalent ($[H^+] = 1.5 \times 10^{-5}$ M) and 10 equivalents ($[H^+] = 1.5 \times 10^{-4}$ M) of acid. The rate constants used in the simulations are shown in table 8.

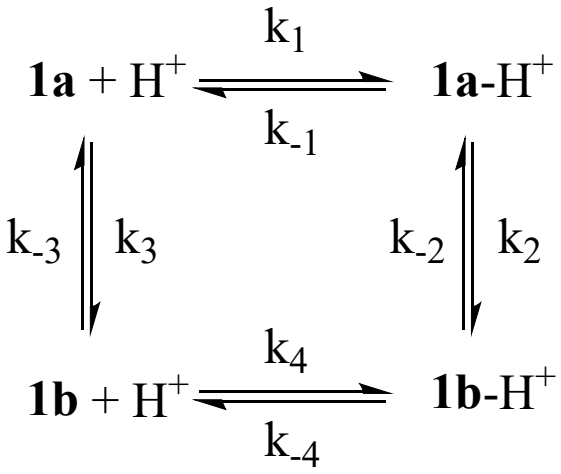

Scheme 5: Network of protonation and deprotonation reactions. The same scheme applies to compound **2a**.

k_{-3} (s^{-1})[e]	4.5×10^{-2}	3.3×10^{-3}
k_4 (M^{-1} s^{-1})[f]	5.0×10^{6}	6.3×10^{5}
k_{-4} (s^{-1})[f]	1.0×10^{-5}	1.0×10^{-5}

Table 8: Rate constants used for the numerical simulations. [a]Values estimated in order to account for a fast protonation process and for the ratio $\frac{k_1}{k_{-1}}$ to match the experimental value determined by spectrophotometric titrations. [b]Experimental values determined from spectrokinetic experiments. [c]Values estimated in order for the ratio $\frac{k_2}{k_{-2}}$ to match the value of 10^3, which is the lowest equilibrium constant that accounts for the fact that the cyclization process converts ≥ 99.9% of the initial open form to the cyclized protonated species. This limiting value is estimated on the basis of absorption coefficient of the open protonated form and the minimum absorbance that can be reliably assessed by the instrument. [d]Values estimated in order for the ratio $\frac{k_3}{k_{-3}}$ to match the value of ≤ 10^{-3} for both compounds.[10a] [e]Values obtained from the experimental data for the ring-opening process. [f]Values that account for a fast protonation process and allow to respect the detailed balance.

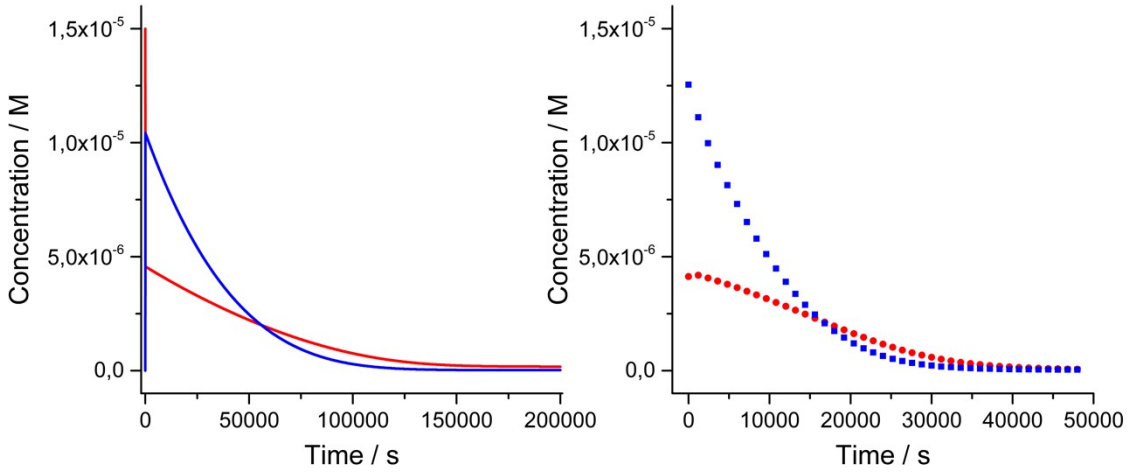

Figure S35: Simulated concentration profile (left) and experimental data (right) for compound **1a** in presence of 1 equivalent of acid. Blue profiles: **1a**-H^+; red profiles: **1a**.

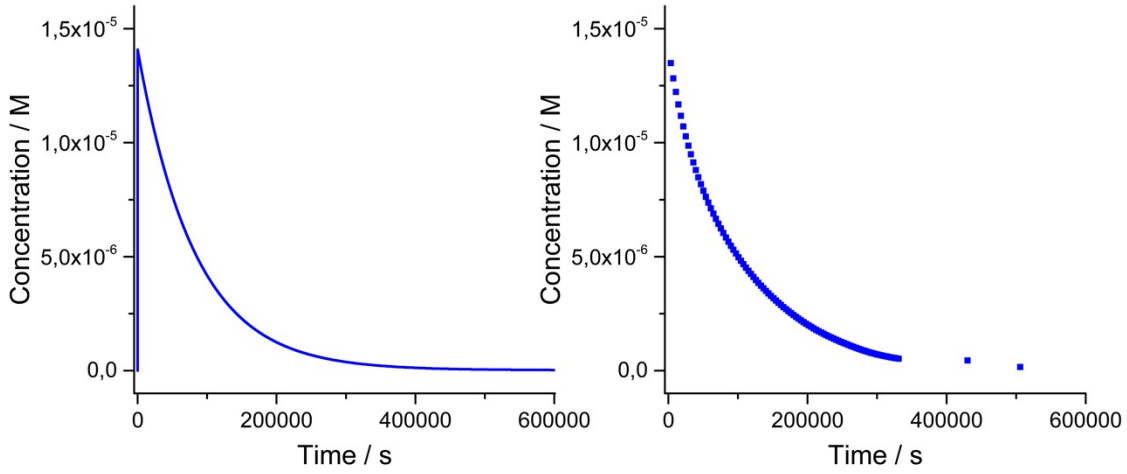

Figure S36: Simulated concentration profile (left) and experimental data (right) for compound **1a**-H^+ obtained by addition of 3 equivalents of acid to **1a**.

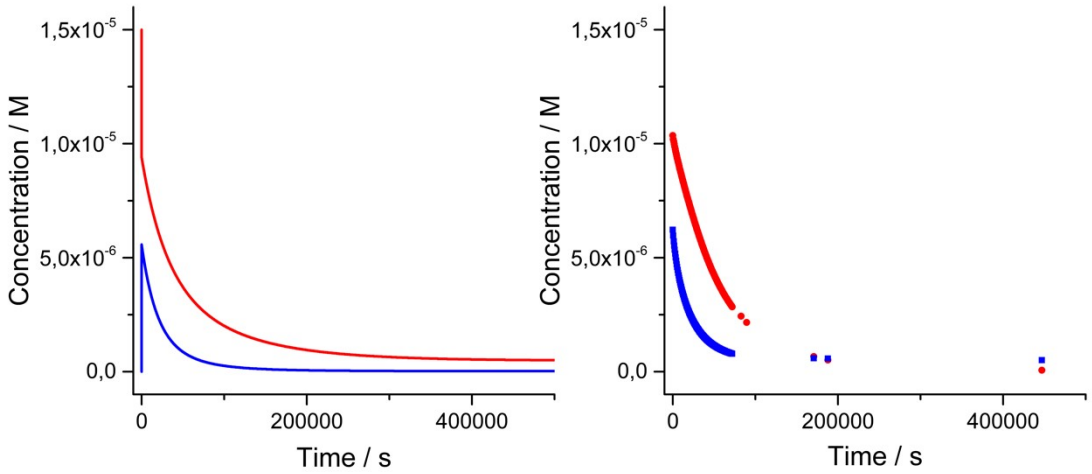

Figure S37: Simulated concentration profile (left) and experimental data (right) for compound **2a** in presence of 1 equivalent of acid. Blue profiles: **2a**-H^+; red profiles: **2a**.

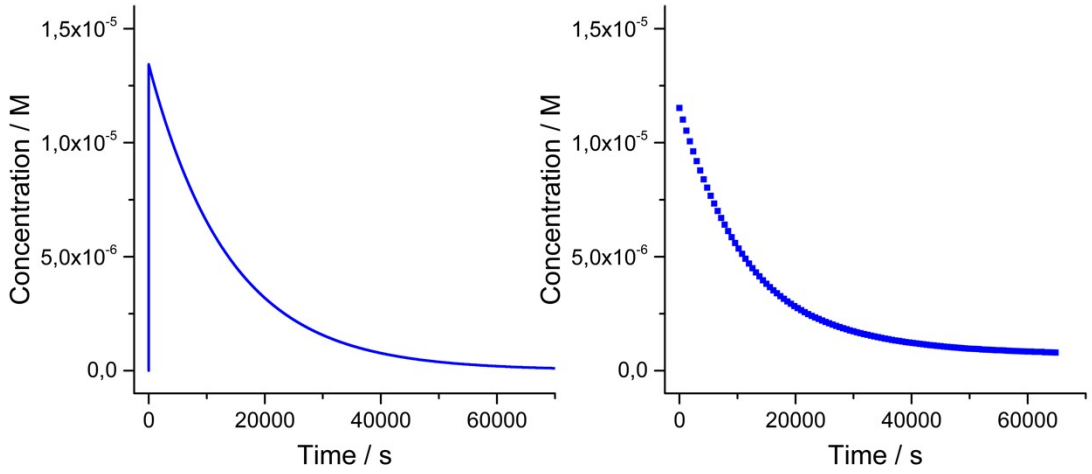

Figure S38: Simulated concentration profile (left) and experimental data (right) for compound **2a**-H^+ obtained by addition of 10 equivalents of acid.

7. NMR Spectra

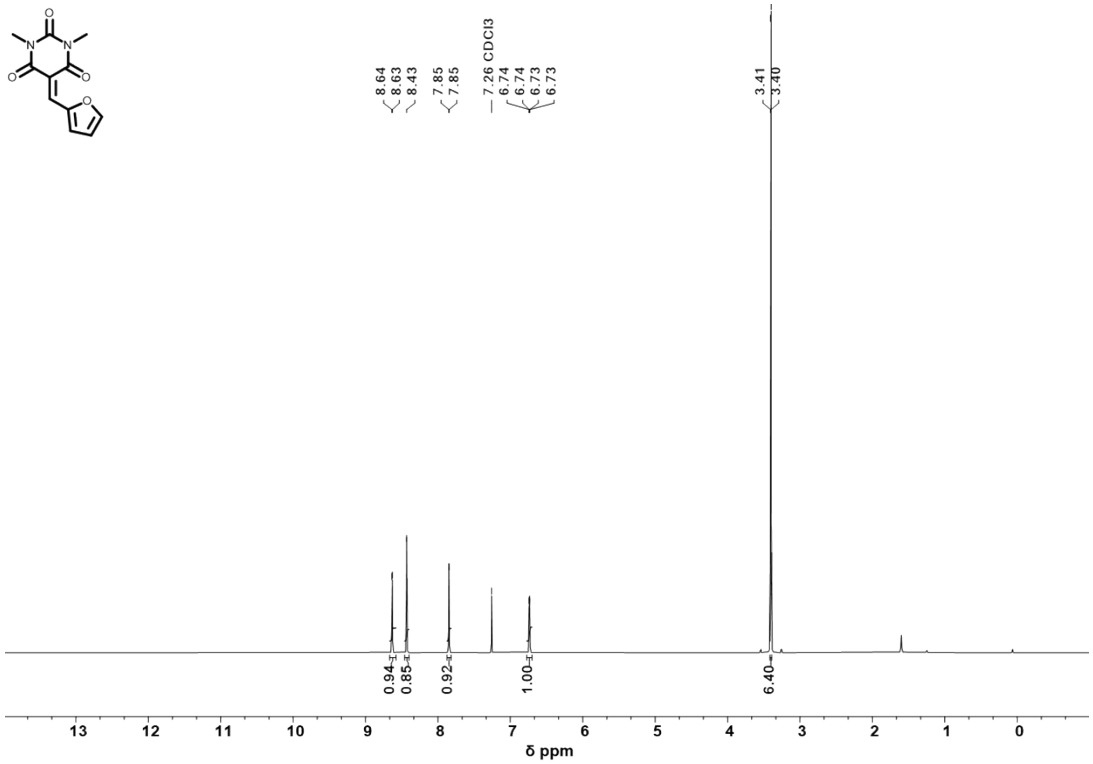

*Figure S39: ^{1}H NMR of acceptor **3**. ^{1}H NMR (500 MHz, CD_2Cl_2, 298 K).*

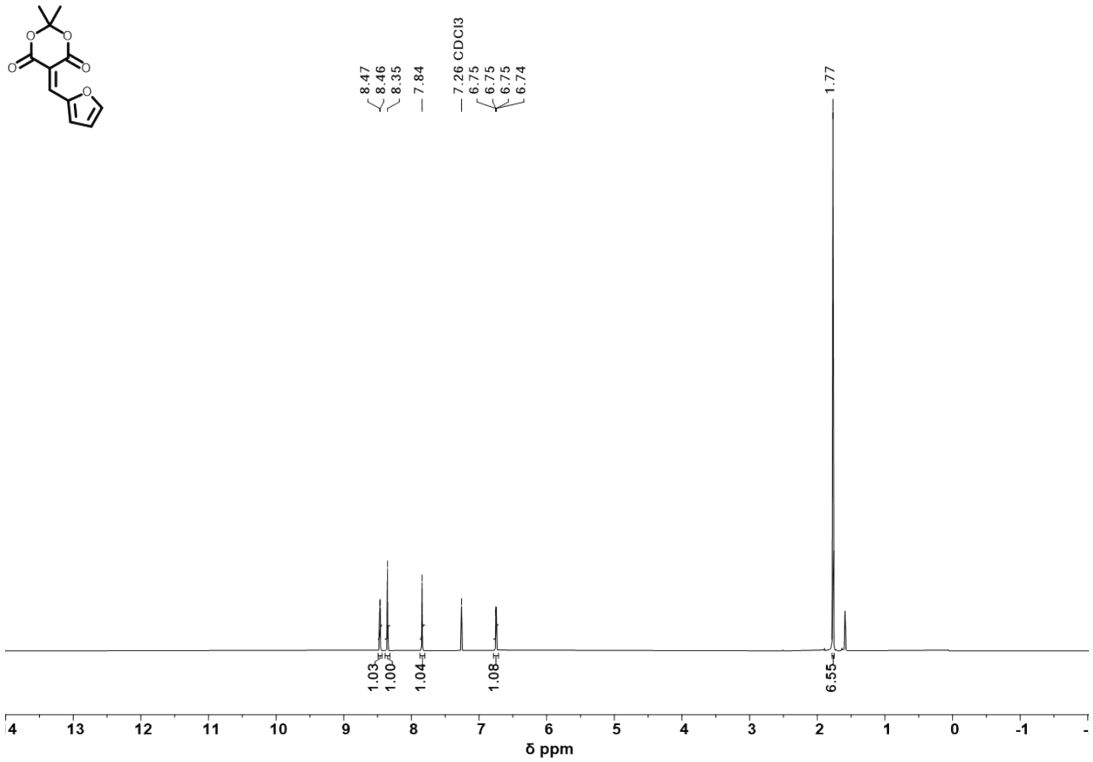

*Figure S40: ^{1}H NMR of acceptor **4**. ^{1}H NMR (500 MHz, CD_2Cl_2, 298 K).*

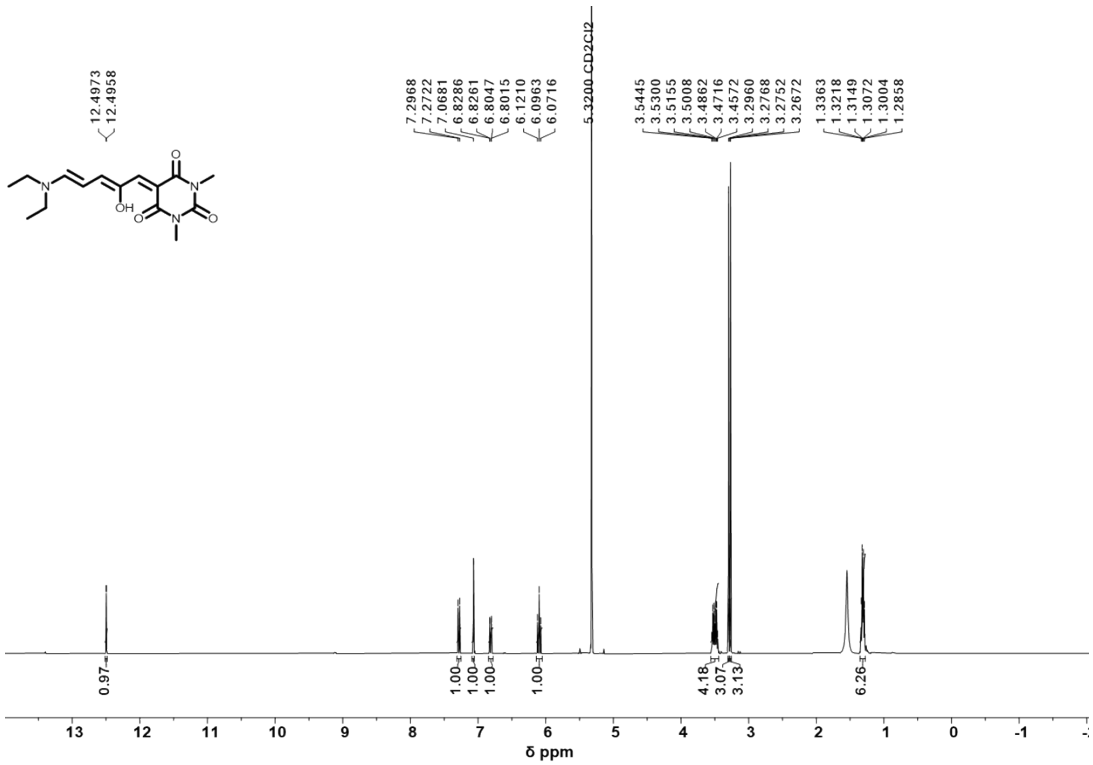

*Figure S41: ^{1}H NMR of DASA **1a**. ^{1}H NMR (500 MHz, CD_2Cl_2, 298 K).*

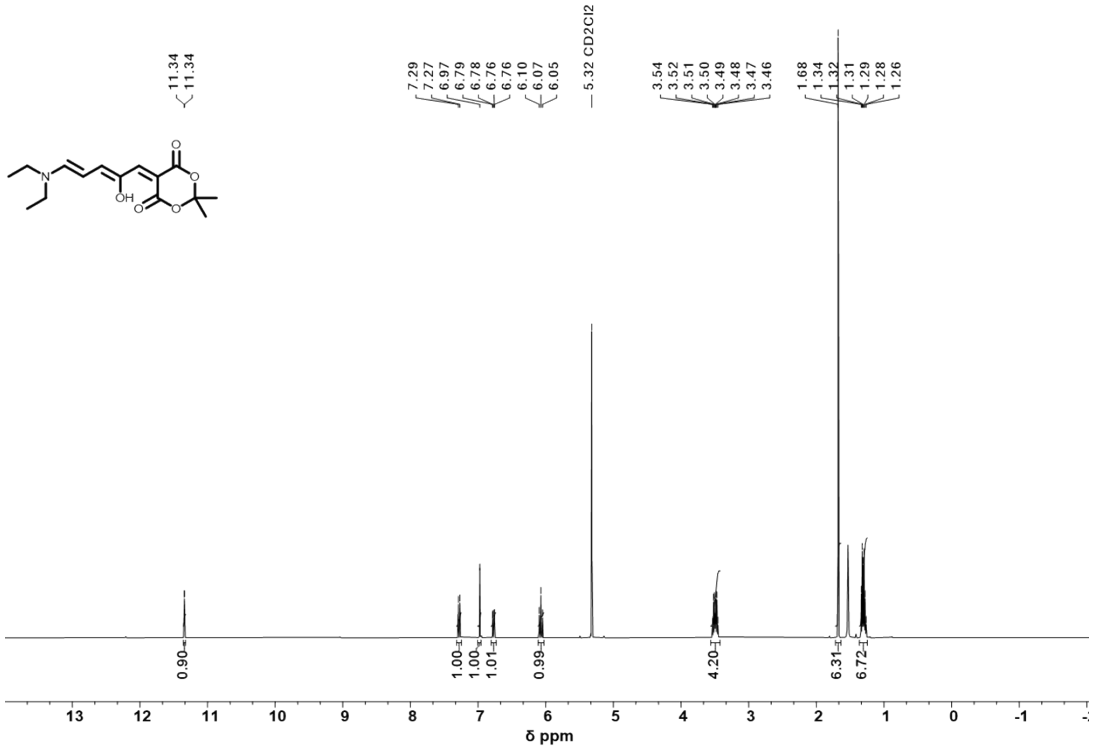

*Figure S42: ^{1}H NMR of DASA **2a**. ^{1}H NMR (500 MHz, CD_2Cl_2, 298 K).*

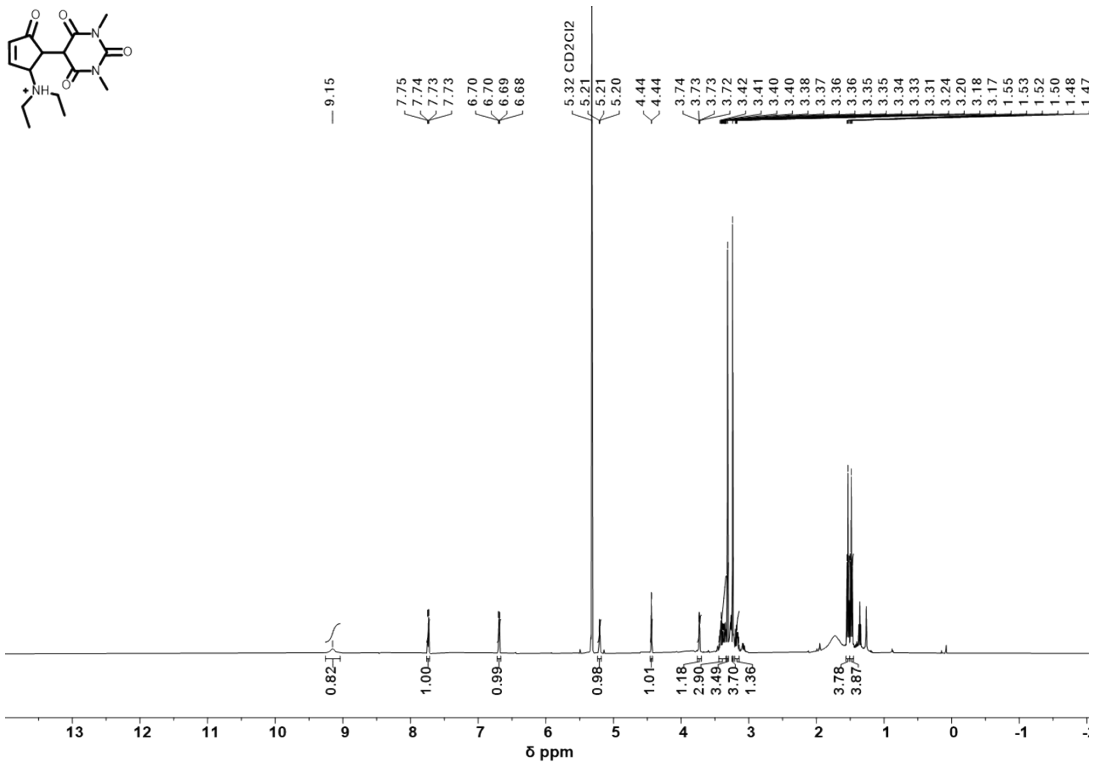

*Figure S43: ^{1}H NMR of DASA **1b**-H⁺. ^{1}H NMR (500 MHz, CD_2Cl_2, 298 K).*

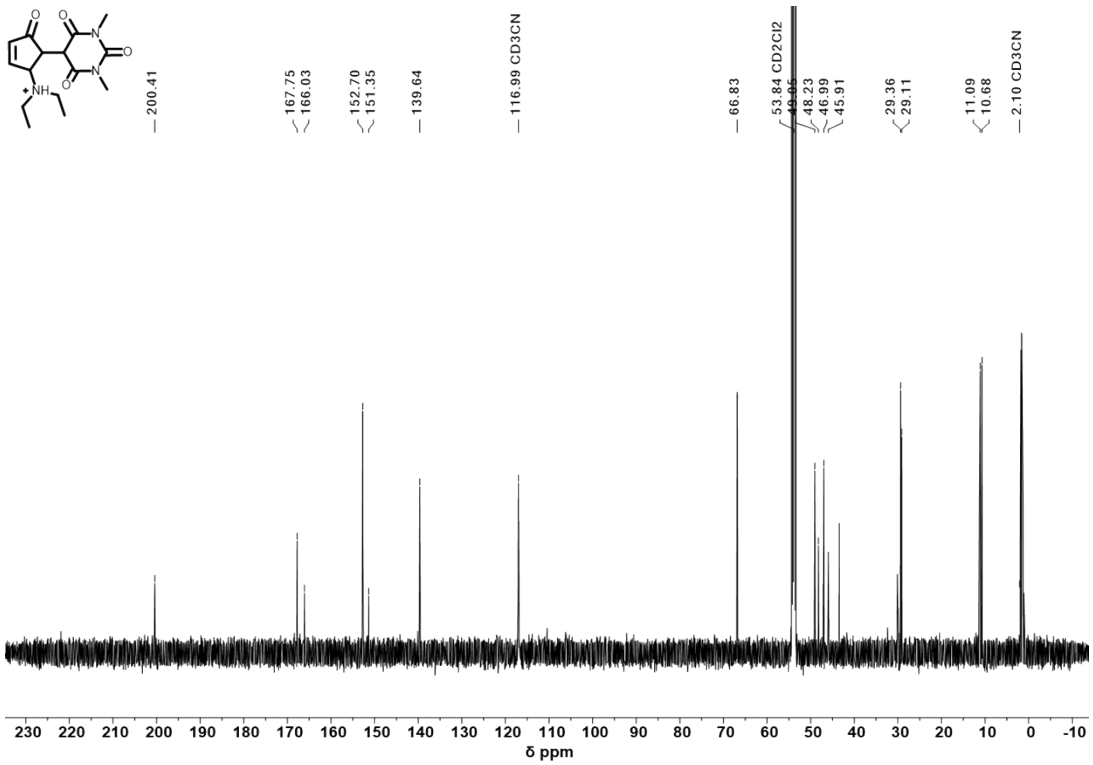

*Figure S44: ^{13}C NMR spectrum of DASA **1b**-H⁺. ^{13}C NMR (126 MHz, CD_2Cl_2, 298 K).*

Signals of deuterated acetonitrile are visible at δ 119 ppm and 2.10 ppm.[11] Deuterated acetonitrile is in the TfOH stock solution, since it is prepared with a mixture of deuterated dichloromethane and deuterated acetonitrile in a 9/1 ratio respectively (*vide supra*).

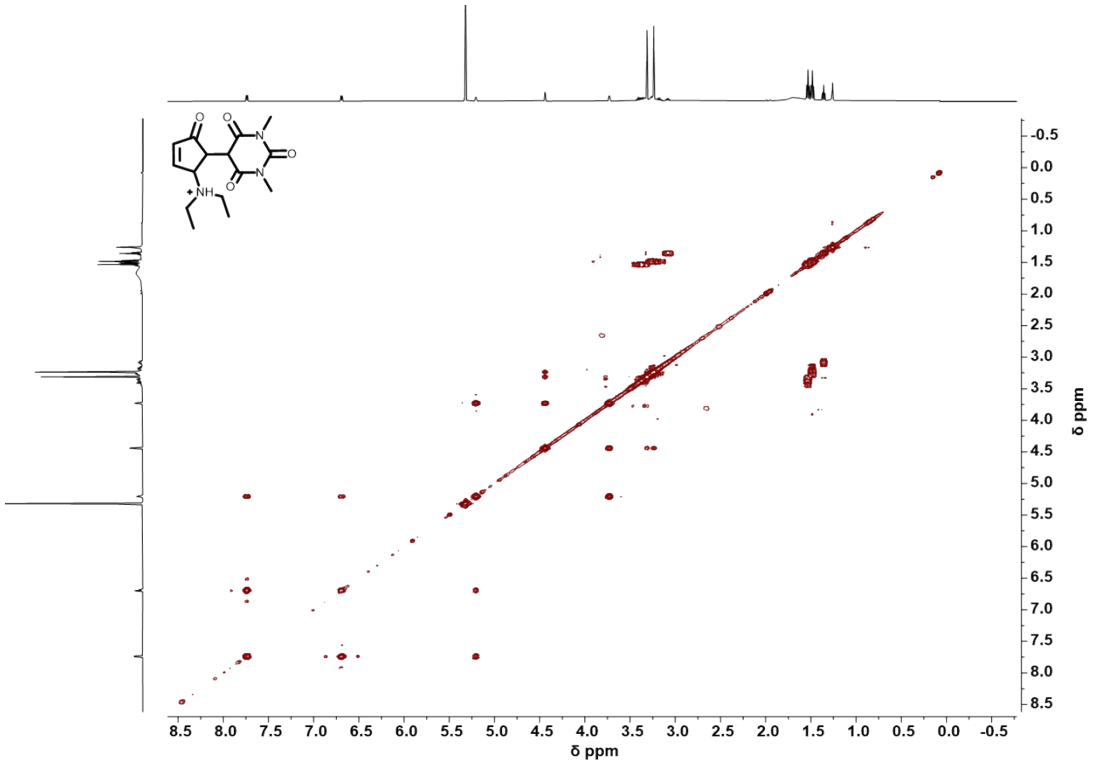

*Figure S45: gCOSY spectra of **1b**-H⁺. (500 MHz, CD_2Cl_2, 298 K).*

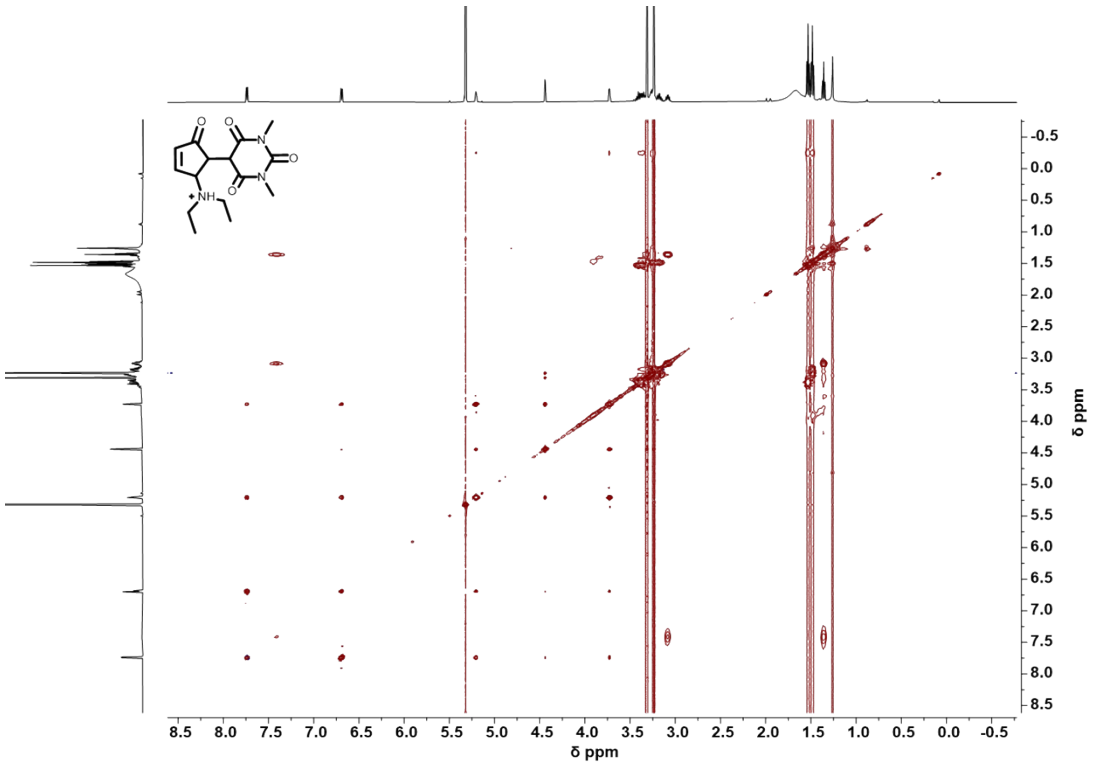

*Figure S46: TOCSY spectra of **1b**-H⁺. (500 MHz, CD_2Cl_2, 298 K, spin lock 80 ms).*

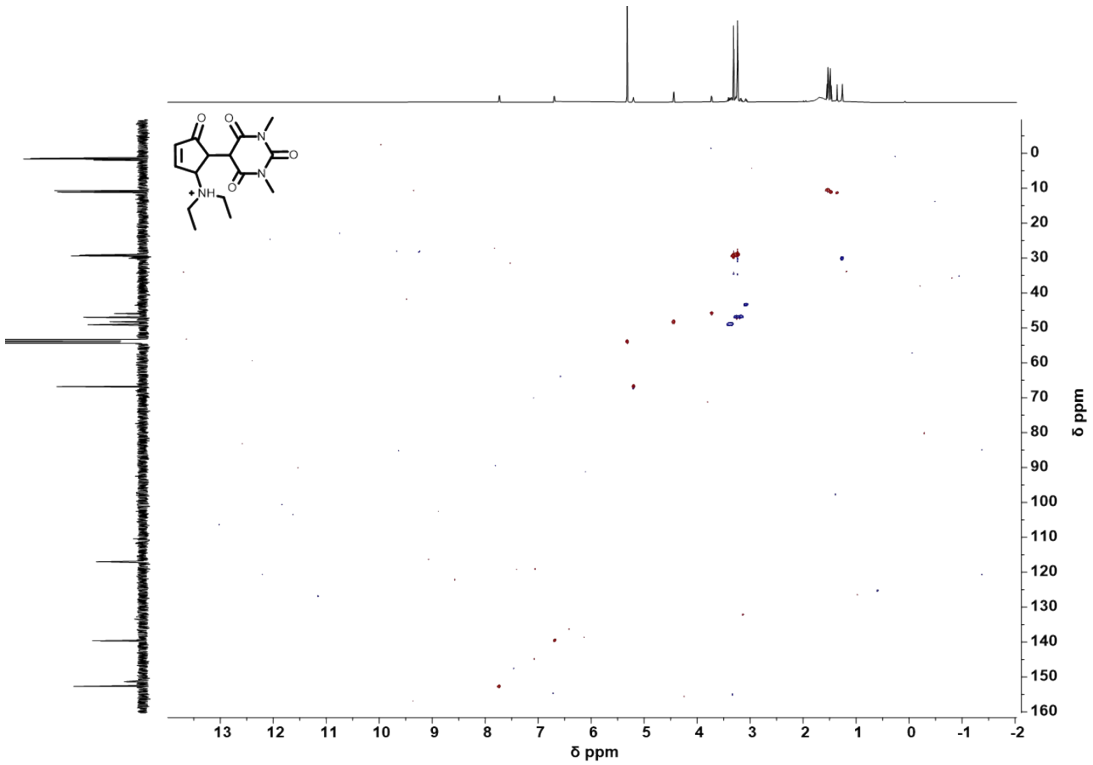

*Figure S47: HSQC spectra of **1b**-H⁺. (500 MHz, CD_2Cl_2, 298 K).*

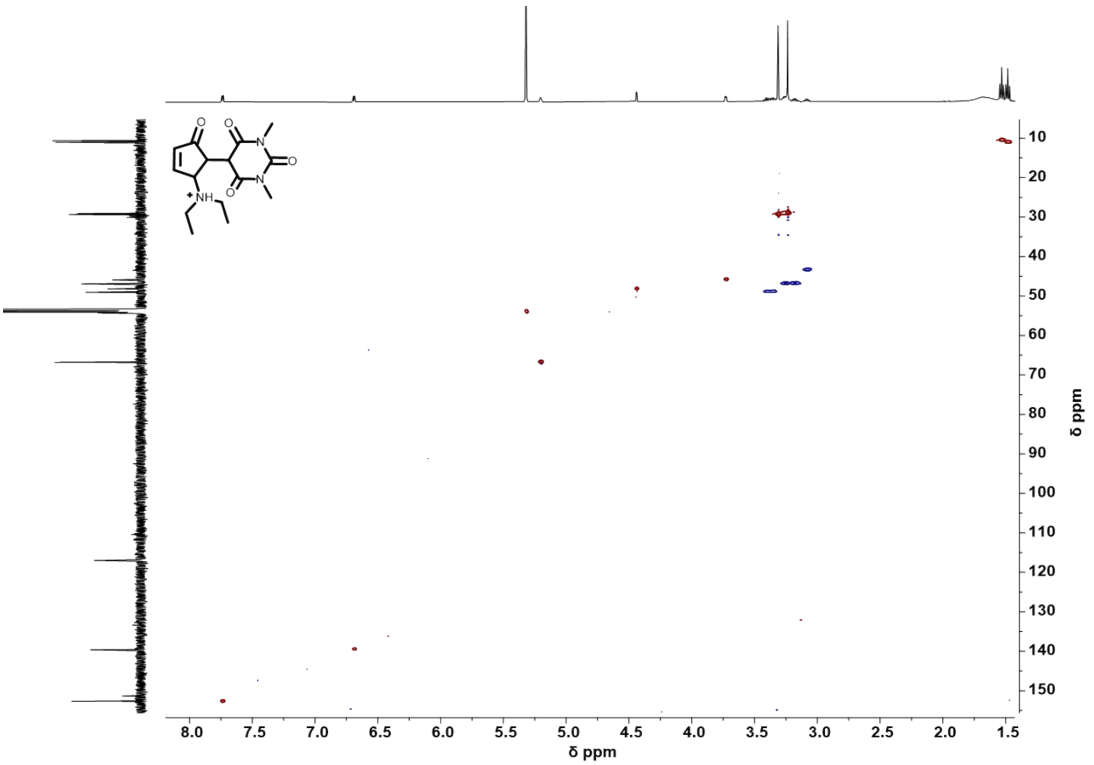

*Figure S48: partial HSQC spectra of **1b**-H⁺. (500 MHz, CD_2Cl_2, 298 K).*

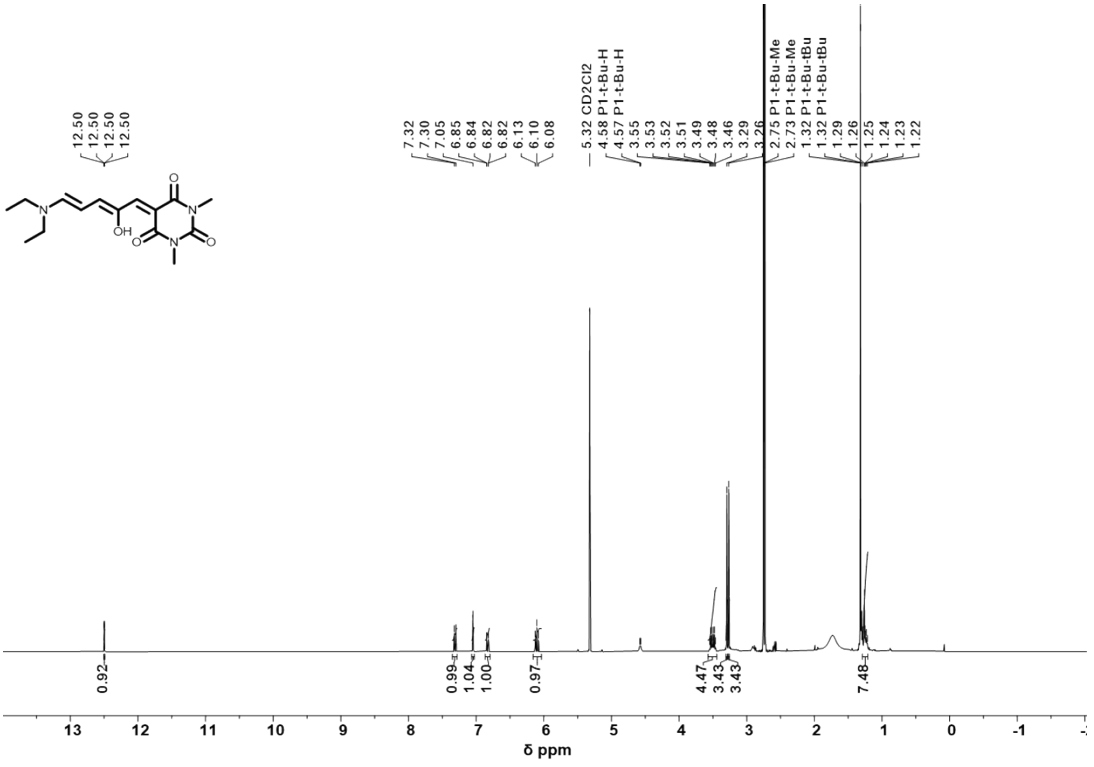

*Figure S49: ^1H NMR spectra of DASA **1a** after treatment of DASA **1b**-H⁺ with 1 equivalent of phosphazene base P1-t-Bu. ^1H NMR (500 MHz, CD_2Cl_2, 298 K).*

Signals corresponding the phosphazene P1-t-Bu base are visible at δ 4.58 ppm protonated P1-t-Bu, 2.75 ppm (s, 9H, Me), 2.73 ppm (s, 9H, Me) and 1.32 ppm (s, 9H, *t*Bu). Integrals were omitted for clarity.

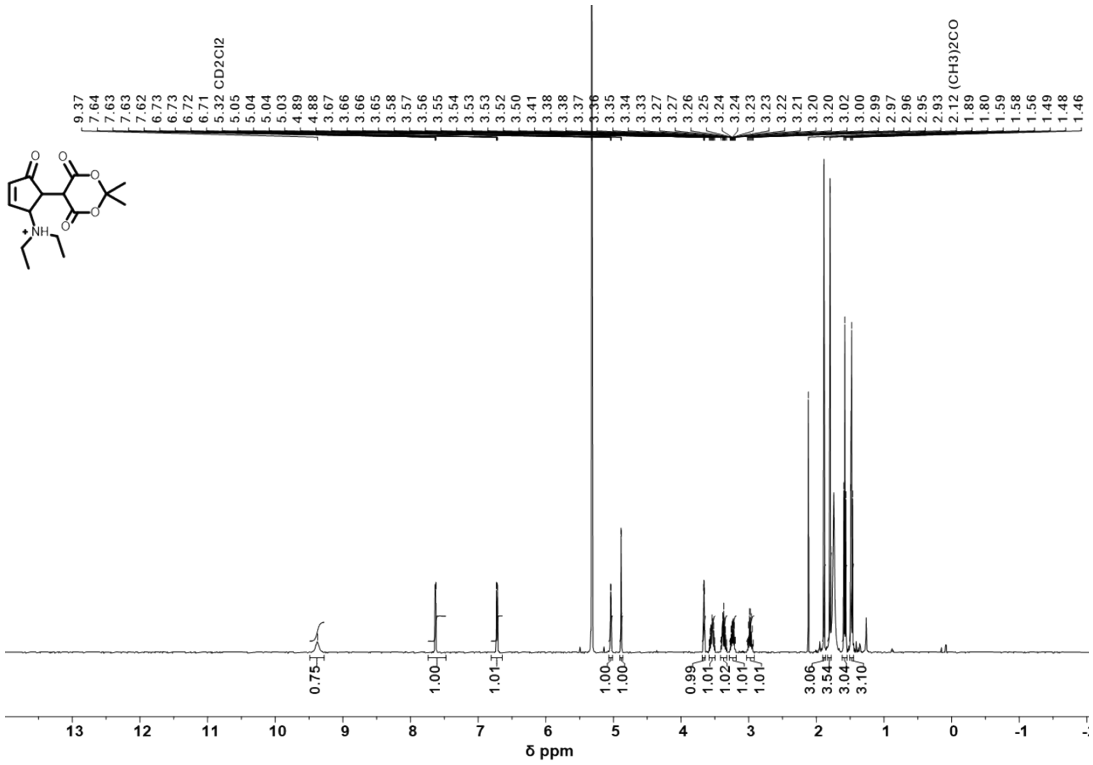

*Figure S50: ^{1}H NMR of DASA **2b**-H$^+$. ^{1}H NMR (500 MHz, CD_2Cl_2, 298 K).*

Acetone signal is visible at δ 2.12 ppm.[11] Generation of acetone when Meldrum's acid derivatives are under acidic conditions has been previously reported in literature.[12]

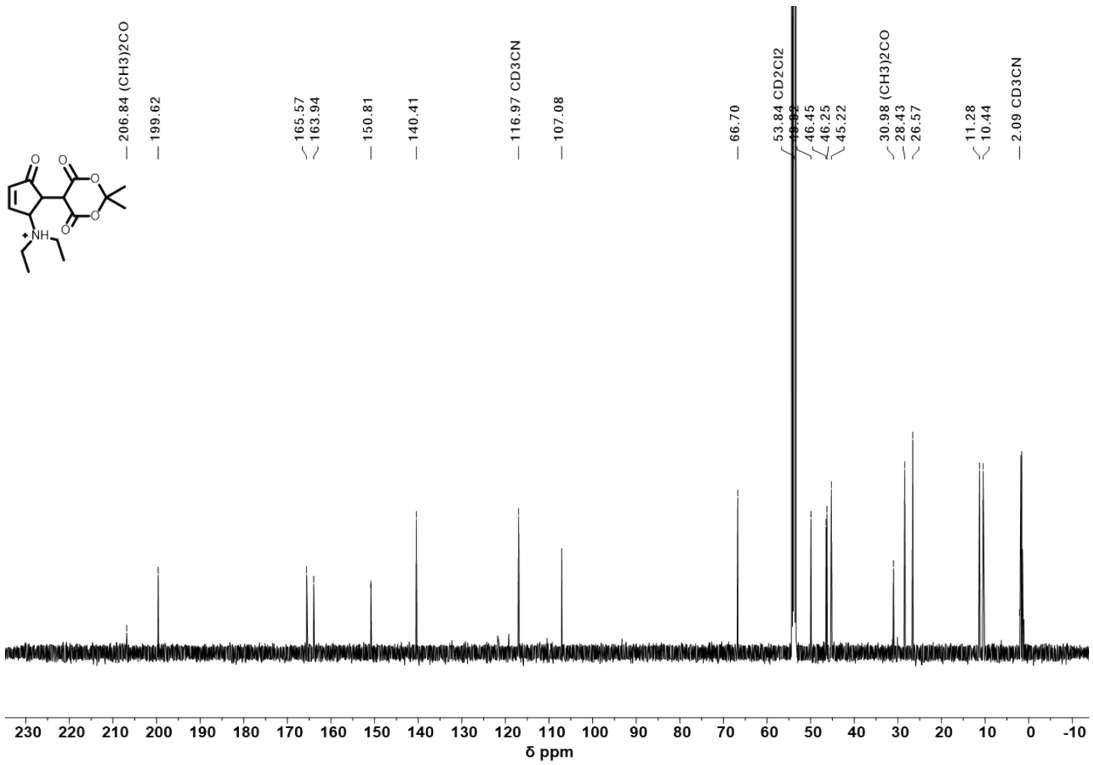

*Figure S51: ^{13}C NMR DASA **2b**-H^+. ^{13}C NMR (126 MHz, CD_2Cl_2, 298 K).*

Acetone signal is visible at δ 206 ppm and 30 ppm. Acetone is generated when Meldrum's acid is under acidic conditions.[12] Generation of acetone when Meldrum's acid derivatives are under acidic conditions has been reported in literature.[12] Signals of deuterated acetonitrile are visible at δ 119 ppm and 2.09 ppm.[11] Deuterated acetonitrile is in the TfOH stock solution, since it is prepared with a mixture of deuterated dichloromethane and deuterated acetonitrile in a 9/1 ratio respectively (*vide supra*).

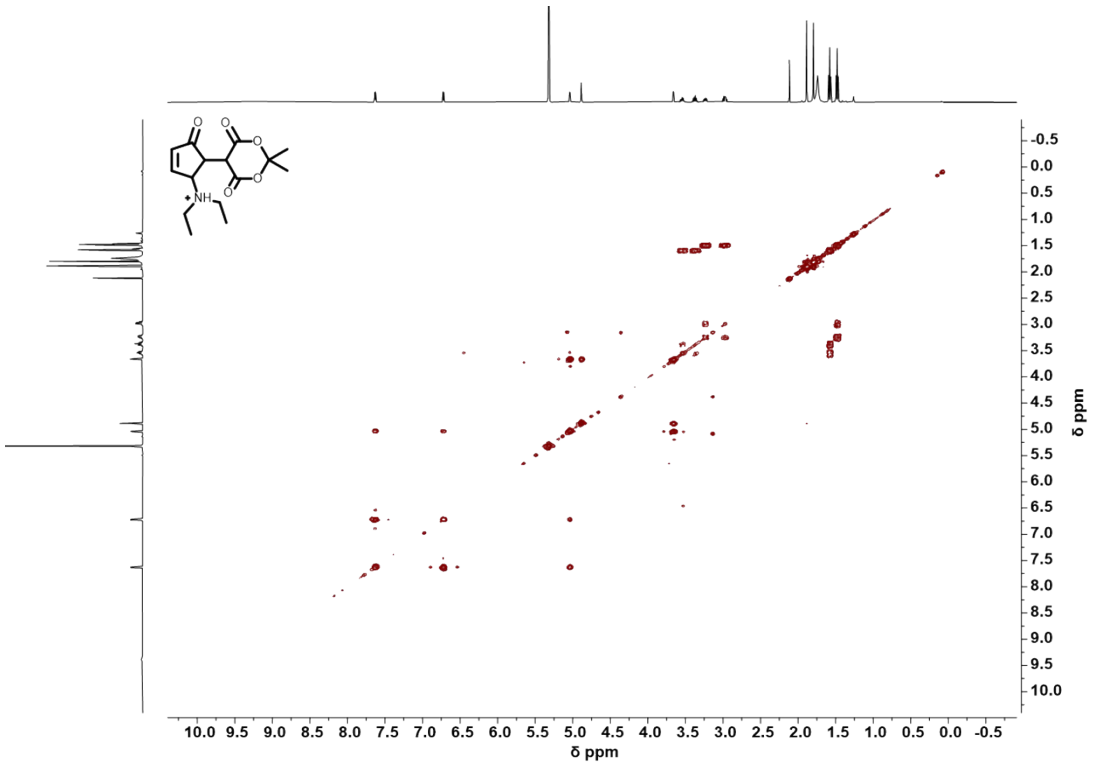

*Figure S52: gCOSY spectra of DASA **2b**-H⁺. (500 MHz, CD_2Cl_2, 298 K).*

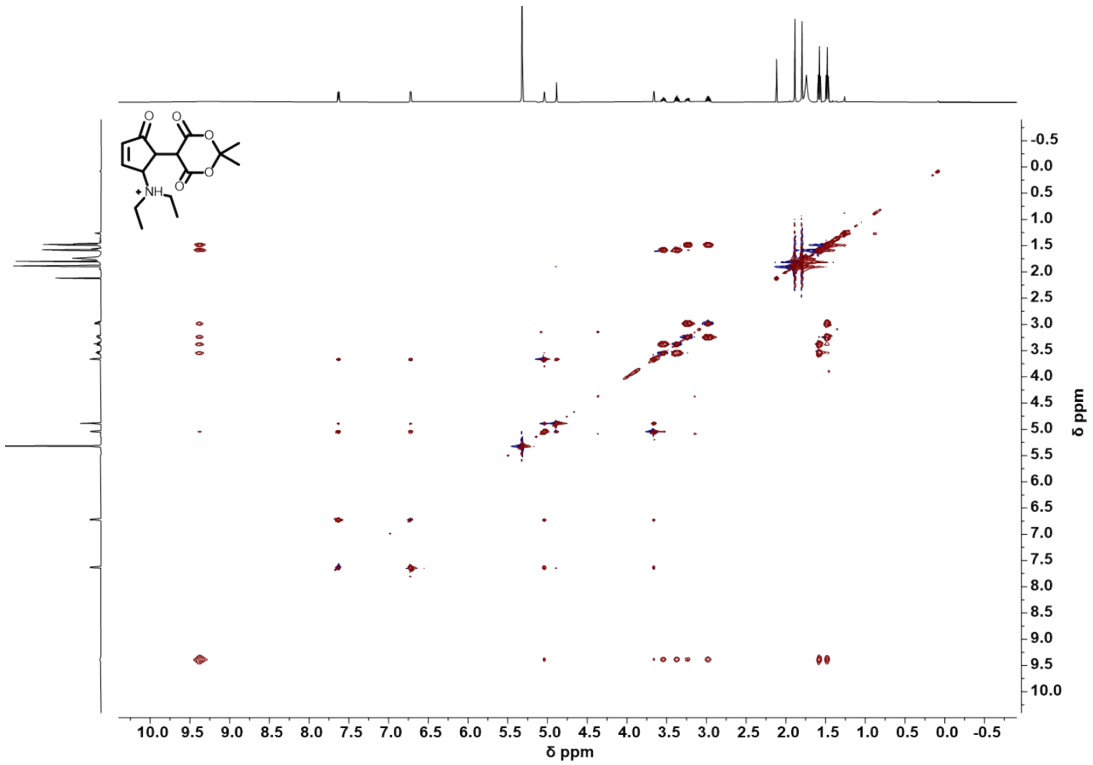

*Figure S53: TOCSY spectra of DASA **2b**-H⁺. (500 MHz, CD_2Cl_2, 298 K, spin lock 80 ms).*

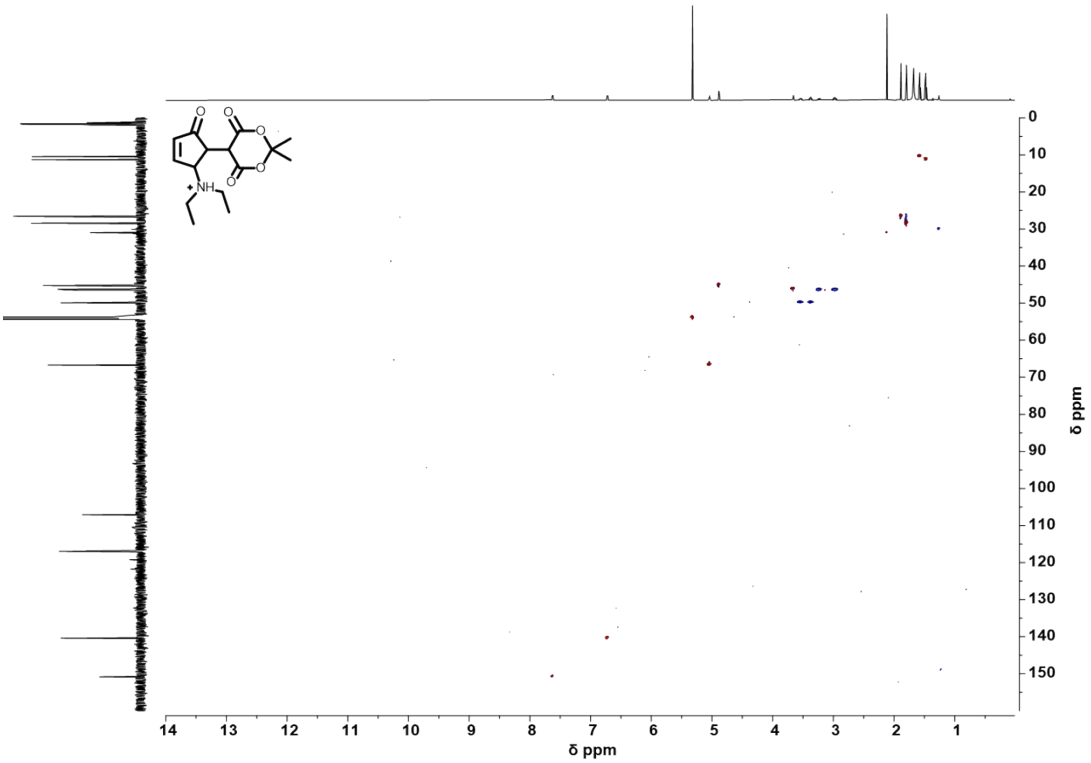

*Figure S54: HSQC spectra of DASA **2b**-H⁺. (500 MHz, CD_2Cl_2, 298 K).*

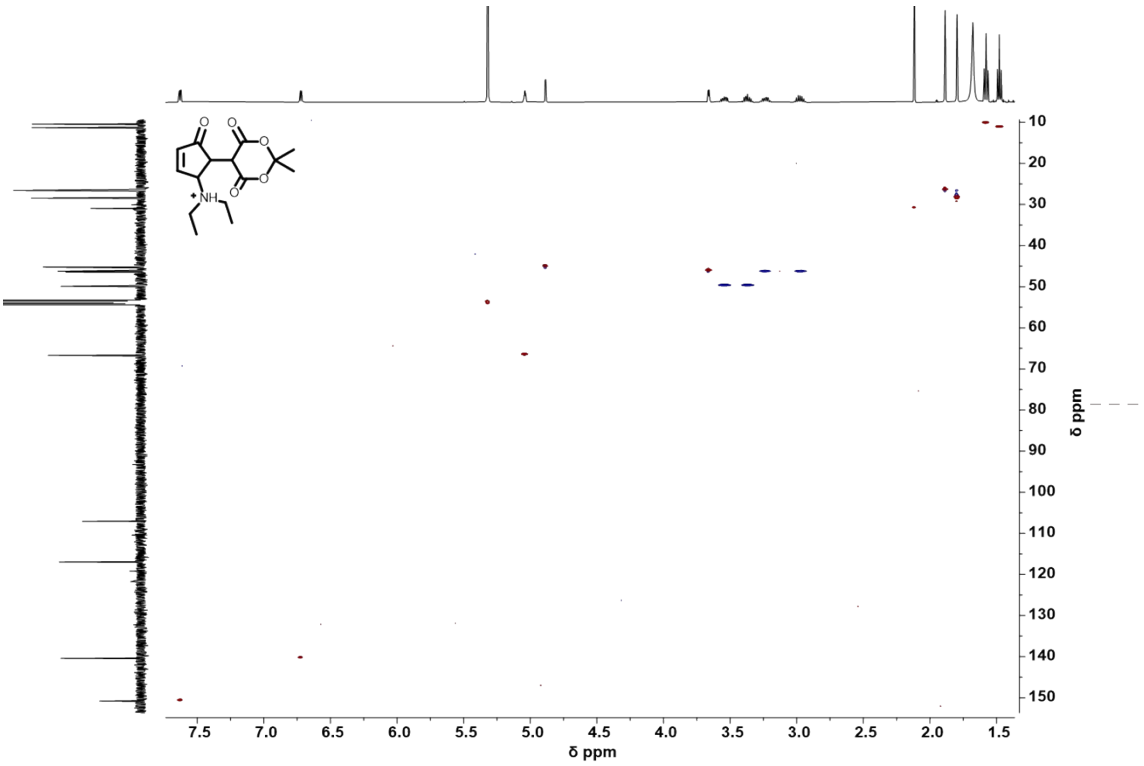

*Figure S55: partial HSQC spectra of DASA **2b**-H⁺. (500 MHz, CD_2Cl_2, 298 K).*

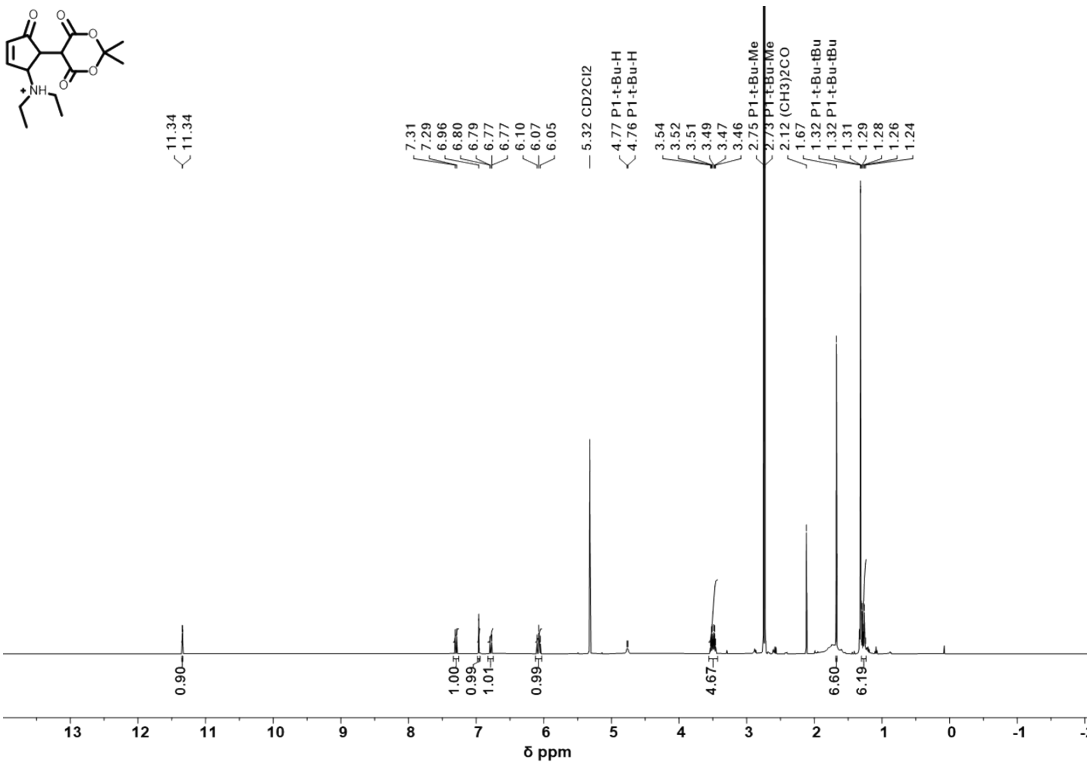

*Figure S56: ^{1}H NMR spectra of DASA **2a** after treatment of DASA **2b**-H$^+$ with 1 equivalent of phosphazene base P1-t-Bu. ^{1}H NMR (500 MHz, CD_2Cl_2, 298 K).*

Acetone signal is visible at δ 2.12 ppm.[11] Generation of acetone when Meldrum's acid derivatives are under acidic conditions has been previously reported in literature.[12] Signals corresponding the phosphazene P1-t-Bu base are visible at δ 4.58 ppm protonated P1-t-Bu, 2.75 ppm (s, 9H, Me), 2.73 ppm (s, 9H, Me) and 1.32 ppm (s,9H, *t*Bu). Integrals were omitted for clarity.

8. References

[1] G. M. Sheldrick, *SADABS, Software for Empirical Absorption Correction*, University of Göttingen, Germany, **1996**.

[2] G. M. Sheldrick, *SHELX97, Program for Crystal Structure Determination*, University of Göttingen, Germany, **1997**.

[3] E. Keller, *SCHAKAL99*, University of Freiburg, Germany, **1999**.

[4] M. Montalti, A. Credi, L. Prodi and M. T. Gandolfi, *Handbook of Photochemistry*, CRC Press, **2006**.

[5] K. Suzuki, A. Kobayashi, S. Kaneko, K. Takehira, T. Yoshihara, H. Ishida, Y. Shiina, S. Oishic and S. Tobita, *Phys. Chem. Chem. Phys.* **2009**, *11*, 9850-9860.

[6] P. Gans, A. Sabatini and A. Vacca, *Talanta* **1996**, *43*, 1739-1753.

[7] R. Radjagobalou, J. F. Blanco, V. D. D. Freitas, C. Supplis, F. Gros, O. Dechy-Cabaret and K. Loubiere, *J. Photochem. Photobiol. A: Chem.* **2019**, *382*.

[8] F. V. Marcoline, J. Furth, S. Nayak, M. Grabe and R. I. Macey, *CPT Pharmacometrics Syst. Pharmacol.* **2021**, *11*, 290-301.

[9] a) S. Helmy, F. A. Leibfarth, S. Oh, S. O. Poelma, C. J. Hawker and J. R. de Alaniz, *J. Am. Chem. Soc.* **2014**, *136*, 8169-8172; b) S. Helmy, S. Oh, F. A. Leibfarth, C. J. Hawker and J. R. de Alaniz, *J. Org. Chem.* **2014**, *79*, 11316-11329.

[10] a) N. Mallo, P. Brown, H. Iranmanesh, T. S. C. MacDonald, M. J. Teusner, J. B. Harper, G. E. Ball and J. E. Beves, *Chem. Commun.* **2016**, *52*, 13576-13579; b) N. Mallo, E. D. Foley, H. Iranmanesh, A. D. W. Kennedy, E. T. Luis, J. Ho, J. B. Harper and J. E. Beves, *Chem. Sci.* **2018**, *9*, 8242-8452.

[11] G. R. Fulmer, A. J. M. Miller, N. H. Sherden, H. E. Gottlieb, A. Nudelman, B. M. Stoltz, J. E. Bercaw and K. I. Goldberg, *Organometallics* **2010**, *29*, 2176-2179.

[12] a) A. M. Dumas and E. Fillion, *Acc. Chem. Res.* **2010**, *43*, 440-454; b) B. H. Mcnab, *Chem. Soc. Rev.* **1978**, *7*, 345-358.